Gas phase dynamics and spectroscopy probed with picosecond transient grating experiments

Todd S. Rose, William L. Wilson, G. Wäckerle,[a] and M. D. Fayer
Department of Chemistry, Standford University, Standford, California 94305

(Received 24 November 1986; accepted 2 January 1987)

Picosecond transient grating experiments in sodium and iodine vapors, involving the $3S \rightarrow 3P$ and $X \rightarrow B$ transitions, respectively, are discussed in detail. Population gratings in sodium demonstrate that the technique can be used to measure velocity distributions in the gas phase. It is shown that the time dependent transient grating signal is related to the Fourier transform of the velocity distribution. Similar experiments on iodine illustrate the effect of state changing collisions on the grating signal. Theoretical calculations for a model in which the change of state is caused by a single collision are given. Close agreement with the data is observed for the situation in which the collision takes the initial velocity into a random velocity distribution. From this model a collision cross section is determined. The results demonstrate that information on collision dynamics can be obtained from grating experiments. In addition, the sodium experiments are used to illustrate a new type of time domain high resolution spectroscopy. When the grating excitation pulses have perpendicular polarizations, a polarization grating, rather than the usual population grating, is formed. Diffraction from the sodium polarization grating shows larger time dependent oscillations in the diffraction efficiency. These oscillations yield the ground state and excited state hyperfine frequencies (1.77 GHz and 189 MHz, respectively). A detailed theoretical description of the origin of the oscillations is presented. The results suggest that polarization grating spectroscopy can have applications in other areas, such as molecular rotational dynamics.

I. INTRODUCTION

In this paper, three different aspects of the application of picosecond transient grating spectroscopy to gas phase systems are presented. First, theory and experiments on very low pressure Na vapor demonstrate that the time dependent transient grating signal can be used to measure the translational motion of atoms and molecules. In fact, the grating signal decay is related to the Fourier transform of the gas velocity distribution. Second, theory and experiments on moderate pressure I_2 vapor illutrate the effects of state changing collisions on the transient grating signal. Analysis of the data leads to a determination of the collision cross section associated with the state change. Finally theory and experiments on Na vapor are used to elucidate a new type of time domain, ultrahigh resolution spectroscopy. The experiments involve the time dependence of a polarization grating. Unlike the more conventional population grating methods, the polarization grating, when applied to Na, displays a time dependent signal with pronounced oscillations at the Na ground state and excited state hyperfine frequencies (1.77 GHz and 189 MHz, respectively).

There are a wide variety of experiments used to probe velocity and collisional effects.[1] Brewer and co-workers[1(a)] employed photon echoes to study grazing collisions. In this work, a single vibration–rotation line was excited with a narrow band laser. The time dependence of the photon echo signal revealed information on the velocity changes produced by collisions which preserved the vibrational–rotation state. There is quantitative agreement between experiment and theory which provides considerable insight into the effects of grazing collisions. Warren[2] is currently using narrow band pump probe experiments to examine velocity changing collisions. In these experiments, a narrow band dye laser is tuned to a frequency in the Doppler profile of a single rovibronic transition. A second dye laser probes the time dependent bleaching at a second frequency in the line. By using pulse sequences with various phases one can obtain various types of information on collisionally induced velocity changes. In these experiments, as well as those which measure Doppler linewidths in equilibrium[3,4] or chemically reacting systems,[4] information on velocity distributions and collisional dynamics is obtained in some manner from the narrow frequency bandwidth of the experiment.

The grating approach is inherently different. It examines the spatial position of molecules as a function of time, and thereby obtains velocity information directly. The measurement of gas phase velocity distributions is analogous to recent grating experiments used to examine exciton transport in crystals,[5,6] and charge carrier transport in hydrogenated amorphous silicon.[7] The grating works in the following manner [see Fig. 1(a)]. Two time coincident picosecond laser pulses of the same wavelength are crossed in the sample. Interference between the two coherently related pulses creates an optical fringe pattern in the sample such that the intensity of light varies sinusoidally in the beam overlap region. The spacing of the interference fringes is determined by the angle between the beams and by the wavelength of the light. When the frequency of the excitation pulses coincides with an absorption band of the gas phase molecule, excited states are produced. These excitations initially will have the same spatial distribution as the sinusoidal optical interfer-

[a] Present address: 2 Physikalisches Institut, der Universität Stuttgart, Pfaffenwaldring 57, 7 Stuttgart 80/Federal Republic of Germany.

 0021-9606/87/105370-22$02.10

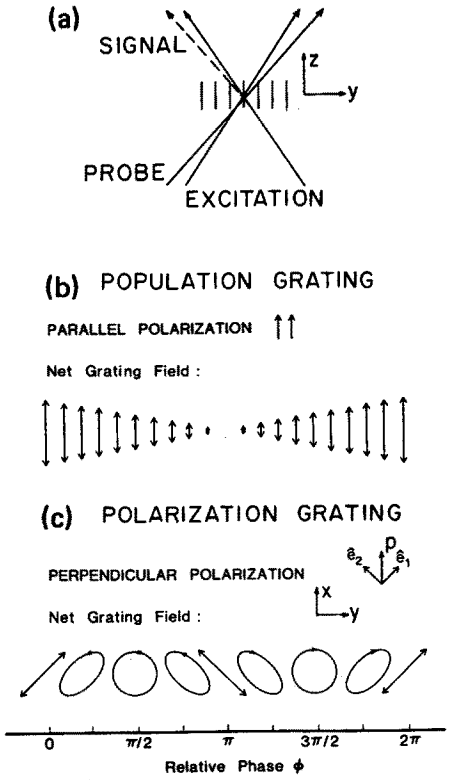

FIG. 1. (a) Transient grating experimental geometry. The excitation pulses, which propagate essentially in the z direction, form a grating with a wave vector along y. The probe pulse is directed into the sample to meet the grating Bragg condition. Part of the probe is diffracted from the grating to give the signal. (b) A population grating is formed by the interference of excitation pulses with parallel polarization. One grating fringe is shown. The electric field amplitude varies sinusoidally along the grating wave vector (y direction). (c) A polarization grating is formed by the vectorial addition of the electric fields of perpendicularly polarized excitation pulses. Again, one grating fringe is shown. The electric field polarization varies from linear to left circular to linear to right circular and finally back to linear across one fringe. The electric field amplitude is constant across the fringe.

ence pattern, i.e., there will be an oscillatory spatial variation in the concentration of excited states. After a suitable time delay, a probe pulse (which may differ in wavelength from the excitation pulses) is directed into the sample along a third path. The probe pulse experiences an inhomogeneous optical medium resulting from the regions of high and low concentrations of excited states. These alternating regions have different indices of refraction, and consequently, a spatially periodic variation in the index of refraction is established. Thus, the probe pulse encounters a Bragg grating which causes it to diffract into one or more orders. [See Fig. 1(a).]

Now consider the effect of the translational motion of excited gas phase molecules. The excited molecules will move from regions of high excited state concentration, grating peaks, to areas of low excited state concentration, grating nulls. The translational motion will fill in the grating nulls and deplete the peaks. Destruction of the grating pattern by spatial redistribution of the excited molecules leads to a decrease in the intensity of the diffracted probe pulse as the probe delay time is increased.[8] Thus, the time dependence of the grating signal is directly determined by the translational motion.

In the Na experiments presented below, the gas is in thermal equilibrium. Therefore the velocity distribution is a Maxwell–Boltzmann distribution, i.e., a Gaussian. The signal decay is the product of an exponential lifetime decay and a Gaussian which is the Fourier transform of the Maxwell–Boltzmann distribution. These experiments demonstrate the feasibility of making fast measurements of velocity distributions without the necessity of observing well resolved spectral lines. The method can be extended to systems which are not in thermal equilibrium. For example, the velocity distributions of fragments from a photodissociation reaction can be examined.

In the I_2 experiments discussed in this paper, the pressure is sufficiently high that there is on the order of one hard sphere collision per I_2 molecule during the time of the experiment. The grating excitation takes place into the middle of the B state vibrational manifold. The initial B state grating has too small a diffraction efficiency to produce a detectable signal at $t = 0$. However, a very strong signal grows in with time. The buildup of signal results from collisions between excited and ground state I_2 molecules which cause the excited molecules to experience a state change. The state that is populated via collisions absorbs the probe strongly, and therefore, gives rise to a large diffraction efficiency. The time dependence of the transient grating signal is a competition between the growth of an observable grating caused by collisions and the destruction of the grating pattern resulting from the translational motion of the molecules. The signal carries information on the initial velocity distribution, the collisional process, and the velocity distribution of those molecules which scatter into the observable state. Detailed theoretical modeling shows that the collision cross section for the state change is somewhat smaller than hard sphere, and that the state changing collision randomizes the initial velocity.

The experiments examining translational and collisional phenomena on Na and I_2 employ population transient gratings. The polarization of the excitation beams are parallel, resulting in an optical interference pattern [Fig. 1(b)]. This interference pattern gives rise to a spatially oscillating concentration of excited states, and therefore a diffraction grating. In another set of Na experiments described below, the excitation beams have perpendicular polarizations which gives rise to a polarization grating [Fig. 1(c)]. Because the optical pulses have perpendicular polarizations, they cannot interfere. The intensity is constant over the excitation region. However, the perpendicular electric fields add vectorially with a phase factor that changes with distance along the grating wave vector. This gives rise to a pattern which varies from lineary polarized light to left circularly polarized light (lcp) to linearly polarized light, to right circularly polarized light (rcp).

The Na $3^2S_{1/2}$ and $3^2P_{3/2,1/2}$ levels are split into manifolds of states by the hyperfine interaction. These splittings give rise to a number of possible transitions with well defined $\Delta M = \pm 1$ selection rules between ground and excited hyperfine states. The $\Delta M = +1$ and the $\Delta M = -1$ transi-

tions are driven by rcp and lcp light, respectively. The signal in the Na polarization grating exhibits oscillations that are characteristic of the ground and excited state hyperfine frequencies. The theoretical analysis presented in this paper demonstrates that the observed oscillations in the grating signal stem from the spatial anisotropy of the excitation conditions. In rcp regions of the grating, superposition states are created by $\Delta M = +1$ transitions. In the lcp grating regions, $\Delta M = -1$ superposition states are generated. In both rcp and lcp grating regions, the absorption probability oscillates at the hyperfine frequencies. The linearly polarized probe encounters a grating with an oscillating diffraction efficiency which gives rise to a modulated diffracted signal intensity. A detailed theoretical analysis shows that the oscillations should vanish for a population grating (parallel excitation polarizations) when certain phase relationships are obeyed.

The unique time behavior of the Na polarization grating is expected to occur whenever there exists manifolds of states with $\Delta M = \pm 1$ selection rules. Hyperfine splittings should be observable in a solid such as Pr^{+3} in LaF_3. In addition, gas phase molecules have rotational states with well defined M values and $\Delta M = \pm 1$ selection rules. Therefore, polarization grating spectroscopy should be useful in the study of the rotational state dephasing.[9]

This paper is organized in the following manner. Section II discusses the theory involving the measurement of gas phase velocity distributions and presents Na experimental results. Section III shows the results for I_2 experiments and discusses the theory concerning the effects of states changing collisions on the grating signal. Section IV returns to Na, and presents theory and experiments on the polarization gratings. Some preliminary aspects of the Na and I_2 experiments have been presented previously.[10,11]

II. GAS PHASE VELOCITY DISTRIBUTIONS: THEORY AND Na POPULATION GRATING EXPERIMENTS

A. Theory

As described in the Introduction, the time dependence of the transient grating signal is directly related to the translational motion of the atoms or molecules. The optical interference pattern generated by crossed excitation pulses is mimicked by the concentration of excited molecules at $t = 0$. As time evolves, the translation of the atoms destroy the grating pattern, and the grating diffraction efficiency is reduced.

For the situation in which a gas is in thermal equilibrium at temperature T, the velocity distribution perpendicular to the grating fringes is given by

$$f(v_y) = \left(\frac{m}{2\pi k_B T}\right)^{1/2} e^{-mv_y^2/2k_BT}. \tag{2.1}$$

In the above equation, y is the grating wave vector direction (see Fig. 1), m is the mass, k_B is the Boltzmann constant, and T is the temperature. Since the grating fringe spacing (1–15 μm) is much smaller than the other dimensions in the problem, (grating height and depth are hundreds of μm) only the motion in the y direction will influence the signal.

At time $t = 0$ the relative concentration of excited molecules at position y is

$$N(y,0) = 1/2(\cos \Delta y + 1), \tag{2.2}$$

where $\Delta = 2\pi/d$ and the fringe spacing $d = \lambda/2 \sin(\theta/2)$.[8] λ is the wavelength of the excitation beams and θ is the angle between them. The grating signal $S(t)$ is determined by the difference between the excited state concentrations of the grating peaks ($y = 0$) and nulls ($y = d/2$) at time t. At any position y, the relative concentration of excited molecules with velocity v_y in the *absence of collisions* is

$$N^{v_y}(y,t) = 1/2[\cos \Delta(y - v_y t) + 1] f(v_y) e^{-t/\tau}, \tag{2.3}$$

where τ is the excited state lifetime and the term $e^{-t/\tau}$ has been added to account for the decay of the grating resulting from population relaxation. It is important to note that the argument of the cosine is indicative of the fact that a molecule with velocity v_y, arriving at point y at time t, initially started at a position $y - v_y t$. To evaluate the peak-null difference in excited state concentration $D(t)$, $N(y,t)$ must be calculated:

$$N(y,t) = \int_{-\infty}^{\infty} N^{v_y}(y,t) dv_y. \tag{2.4}$$

The signal $S(t)$ is proportional to $[D(t)]^2$. Consequently,

$$S(t) = A[D(t)]^2 = A[N(0,t) - N(d/2,t)]^2. \tag{2.5}$$

Substituting Eq. (2.3) into Eq. (2.4) and then substituting this result into Eq. (2.5) yields

$$S(t) = A\left[e^{-t/\tau} \int_{-\infty}^{+\infty} f(v_y)\cos(\Delta v_y t) dv_y\right]^2. \tag{2.6}$$

Equation (2.6) is a general result for any velocity distribution $f(v_y)$ when the time scale of the measurement (a few nanoseconds) is fast compared to the collision time. The integral is the cosine Fourier transform of the velocity distribution $f(v_y)$. The signal $S(t)$ is proportional to the square of the Fourier transform of the velocity distribution multiplied by the square of the population relaxation term.

For a velocity distribution $f(v_y)$ described by Eq. (2.1), Eq. (2.6) becomes

$$S(t) = A\, e^{-(\Delta t)^2 k_B T/m}\, e^{-2t/\tau}. \tag{2.7}$$

Equation (2.7) shows that a Gaussian velocity distribution yields a signal which is the product of a Gaussian and an experimental term. By changing Δ (changing the fringe spacing), one can scale the time such that different portions of the velocity distribution are emphasized on the experimental time scale.

B. Experimental procedure

In the sodium experiments tunable pulses were generated by synchronously pumping two dye lasers with the second harmonic of an acousto-optically Q-switched and modelocked Nd:YAG laser. The output of one dye laser was used to produce the excitation pulses, while that of the other was used to generate the probe. Thus, the probe and excitations could be independently tuned into the upper or lower sodium D lines at 589.0 ($^2P_{3/2}$) and 589.6 nm ($^2P_{1/2}$). The tunable pulses were 18 ps in duration, had a bandwidth of 0.7

cm^{-1}, and were attenuated to ~ 100 nJ and $\sim 0.5\,\mu$J for the excitation and probe, respectively. The spot sizes were 200 μm. The excitation pulses had parallel polarizations to form a population grating (Fig. 1).

The diffracted signal was detected by a cooled phototube and sent into a lock-in amplifier. The probe was delayed from the time coincident excitation pulses with a motor driven delay line which generated a voltage proportional to the delay. A small computer was used to digitize the output of the lock-in amplifier and the delay line voltage. In this manner the time dependent curves were stored for subsequent analysis.

The Na sample was contained within a 3 cm long optical cell with 1 cm diam windows. The cell temperature was controlled by the voltage applied to heating wire wrapped around the cell. There was an independently heated side arm which was used to control the Na pressure at about 2×10^{-7} Torr.[12] The cell temperature was measured by a resistance thermometer in contact with the body of the cell. It is interesting to calculate the total number of atoms that contributed to the signal. If the temperature of the main part of the cell is 600 K and the vapor pressure is 2×10^{-7} Torr, the density is 3.2×10^{9} atom/cm^3. For a fringe spacing of 12 μm and a beam diameter of 200 μm, the grating volume is approximately 3×10^{8} μm^3. The number of atoms within this volume is $\sim 10^{6}$.

C. Results and discussion

Figure 2 displays transient grating data taken on Na vapor at ~ 600 K with the excitation wavelength tuned to the $^2P_{3/2}$ manifold and the probe wavelength tuned to the $^2P_{1/2}$ manifold. The curve exhibits a nonexponential decay. At very short time (<1 ns) there is a large coherence artifact arising from the macroscopic polarization which is initially produced upon excitation. This polarization decays on the time scale of the free-induction decay associated with the Dopper linewidth. For Na at 600 K, the Doppler linewidth is 6.2×10^{-2} cm^{-1}, which corresponds to a decay time of approximately 0.5 ns. Following the decay of the macroscopic polarization, the transient grating decays because of population relaxation (fluorescence) and the translational motion of the atoms. The fluorescence lifetime in the absence of collisions is 16 ns.[13]

The curve through the data in Fig. 2 is the best single parameter fit to Eq. (2.7). The fringe spacing is 12.2 μm, $\tau = 16$ ns, and m is the mass of Na in grams. The single adjustable parameter is the temperature T. The calculated curve has $T_f = 590$ K as compared to the approximate sample temperature of 585 K measured by the thermometer in contact with the optical cell wall. After the initial coherence artifact, the shape of the calculated curve is in excellent agreement with the data.

Figure 3 shows the same grating decay as in Fig. 2, as well as those taken at different fringe spacings, namely 5.3 and 6.8 μm, and with different experimental conditions (i.e., wavelengths of probe and excitation and temperature). Note

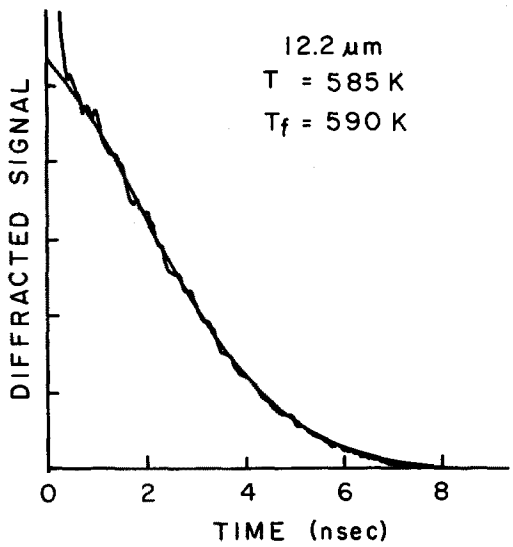

FIG. 2. Na population grating. The signal intensity is plotted vs the probe delay time. The probe and excitations are tuned into the $^2P_{1/2}$ (589.6 nm) and $^2P_{3/2}$ (589.0 nm) manifolds, respectively. The fringe spacing of the grating is 12.2 μm and the temperature T (measured by a resistance thermometer) is 585 K. The solid line is the theoretical fit to data obtained from Eq. (2.7). The fringe spacing is set at 12.2 μm, while the lifetime is fixed at 16 ns. The adjustable parameter, the temperature T_f is in agreement with the measured temperature.

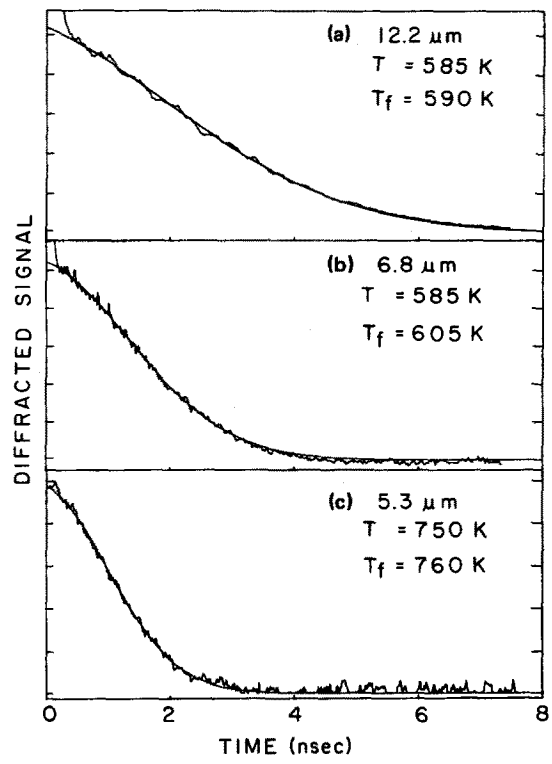

FIG. 3. Comparison of Na experimental data (taken under different conditions) to theoretical fits obtained from Eq. (2.7). T and T_f are the measured and fit temperatures. λ_p = probe wavelength; λ_{exc} = excitation wavelength. (a) Fringe spacing = 12.2 μm. $\lambda_p = 589.6$ nm ($^2P_{1/2}$); $\lambda_{exc} = 589.0$ nm ($^2P_{3/2}$). $T = 585$ K; $T_f = 590$ K. (b) Fringe spacing = 6.8 μm. $\lambda_p = \lambda_{exc} = 589.6$ nm ($^2P_{1/2}$). $T = 585$ K; $T_f = 605$ K. (c) Fringe spacing = 5.3 μm. $\lambda_p = \lambda_{exc} = 589.6$ nm ($^2P_{1/2}$). $T = 750$ K; $T_f = 760$ K.

that as the fringe spacing becomes smaller, the time required for atoms to move from grating peaks to nulls is decreased, and therefore the decay of the signal is faster. As can be seen in Eq. (2.7), the time is scaled by the inverse of the fringe spacing. As the fringe spacing becomes smaller, the Gaussian term will increasingly dominate the lifetime exponential. The theoretical fits drawn through the data in Fig. 3 for fringe spacings of 12.2, 6.8, and 5.3 μm have temperatures (T_f) of 590, 605, and 760 K, respectively. The corresponding temperatures measured by the resistance thermometer (T) are 585, 585, and 750 K. Thus, there is excellent agreement between theory and experiment over this range of fringe spacings. It should be mentioned that deviations from the expected results were found to occur at fringe spacings significantly smaller than 5.3 μm because of interference from the coherence spike and at fringe spacings greater than 20 μm because of boundary effects. This latter consideration involves the fact that at large fringe spacings, the Gaussian intensity profile of the laser beams becomes an important factor since there are only a few fringes inside the grating region.

Figures 2 and 3 demonstrate that gas phase velocity distributions can be directly examined with the transient grating approach. It is not necessary to have high resolution or a well resolved spectrum. The measurement is made by direct observation of the translational motion of the atoms or molecules against a well-defined distance scale provided by the grating fringe spacing. The Na experiments [which are quantitatively described by Eq. (2.7)] illustrate the situation of thermal equilibrium in which there are no collisions on the time scale of the experiment, i.e, a few nanoseconds. If a system is initially created with a nonequilibrium velocity distribution, velocity changing collisions will bring the system into thermal equlibrium. (The collisions discussed here do not change the electronic or vibronic state of the atoms or molecules. State changing collisions of this nature are discussed in Sec. III.) If the time scale of the velocity changing collisions is long compared to the experimental time scale, the grating experiment can be used to follow the time evolution of the velocity distribution function. If velocity changing collisions occur on a time scale which is fast compared to the experimental time frame, then the velocity of any particle will be randomized well before it travels a distance equivalent to the grating fringe spacing. (The mean free path of the particle is much smaller than the fringe spacing.) In this situation, transport is diffusive on the distance scale of the experiment. For diffusive transport, the grating signal decays as[5]

$$S(t) = A\, e^{-2\Delta^2 D t}\, e^{-2t/\tau}. \tag{2.8}$$

The decay is exponential with the transport term again multiplied by an exponential population decay term. Δ and τ have been previously defined, and D is the diffusion constant. For a thermal equilibrium system,

$$D = 2/3\left[(k_B^3 T^3/m\pi)^{1/2}/\sigma P\right], \tag{2.9}$$

where P is the pressure and σ is the collision cross section.[14] The other parameters have been defined earlier.

III. STATE CHANGING COLLISIONS: I_2 POPULATION GRATING EXPERIMENTS AND THEORY

A. Experimental procedure

Transient population grating experiments were conducted on I_2 vapor at moderate pressure. The general experimental setup was similar to that discussed earlier. Tunable 30 ps, 10 μJ dye pulses were beam split and crossed to form the grating. The excitation pulses were tuned to 560 nm. The probe pulse was obtained by doubling the output of the Nd:YAG laser. The resultant 532 nm pulse was 80 ps long and 5 μJ in energy. The excitation and probe bandwidths were $\sim$10 and $\sim$1/3 cm^{-1}, respectively. Spot sizes were about 250 μm. The sample was I_2 vapor in a 1 cm length evacuated cell which was wrapped with heating wire. The temperature of the cell was held at 430 K. The I_2 pressure was maintained at approximately 16 Torr by controlling the temperature of a side arm.[15]

Figure 4 shows transient grating data taken with a large (15 μm) fringe spacing. At this large fringe spacing, translational motion has little effect on the signal. The grating time dependence results from population kinetics. The signal is seen to have $\sim$0 intensity at $t = 0$ and to grow rapidly with time. This is in contrast to Fig. 3 in which the Na data displays the time dependence of collision free translational motion and excited state decay. The 560 nm excitation wavelength causes transitions from the ground state $X(^1\Sigma_g^+)$ to $V \approx 19$ vibrational level of the B ($^3\pi_{0^+u}$) state. The 532 nm probe corresponds to a transition from the X state to $V \approx 31$ of the B state.[16,17] In the absence of collisionally induced state changes, the probe should experience a maximum grating diffraction efficiency at $t = 0$. The fact that a strong increasing signal is observed, demonstrates that the state being probed is not the initially prepared excited state, but rather a state which interacts strongly with the probe radiation field at 532 nm. (Since the absorption from the X state at 532 nm is weak,[18] the signal from this transition is extremely small[8] and consequently not detected.) At the temperature and

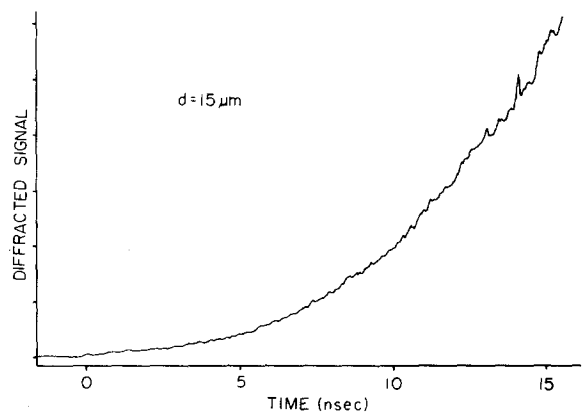

FIG. 4. Transient grating signal obtained from I_2 with a fringe spacing of 15 μm. At large fringe spacings the decay of the grating resulting from molecular motion is minimal on the experimental time scale. Thus, in this regime, the grating examines population kinetics. Unlike Figs. 2 and 3, the I_2 data display a buildup of signal rather than a decay. State changing collisions populate the "observable state" and give rise to the time dependence of the signal.

pressure of the experiment, the I_2 molecules will experience a small number of hard sphere collisions on the experimental time scale. These collisions must cause state changes to another electronic state or to a different region of the vibrational manifold of the B state. The new state formed cannot be a dissociative state since the rising signal implies a buildup of population. Furthermore, iodine atoms do not absorb the 532 nm probe.

To see if a reasonable number of collisions occur on the time scale of the experiment, one can calculate a hard sphere collision frequency[19] for I_2 at 16 Torr and 430 K. If the hard sphere collision parameter d_c is set equal to twice the I_2 bond length (2.66 Å),[18] the average hard sphere collision time is ~ 12 ns. Consequently, a significant number of I_2 molecules can undergo at least one hard sphere collision.

Figure 5 displays fringe spacing dependent data. Except for different fringe spacings, the conditions for each data set are identical. As the fringe spacing is decreased, the destruction of grating pattern by molecular translations becomes increasingly important. The rapid rise in signal is damped by the Gaussian decay produced by the distribution of molecular velocities.

Physically the situation is as follows. A fringe pattern of excited states is produced at $t = 0$. However, the resulting grating interacts so weakly with the probe pulse that the grating has essentially zero diffraction efficiency. Therefore, the initial grating is not observable. Nonetheless, as time proceeds, the translational motion begins to smear out the grating and collisions occur. The collisions take some molecules from the initial ensemble to a new state (or states) which interacts strongly with the probe pulse. Molecules in the new state form the observable ensemble. If collisions occur before the grating pattern is destroyed by motion in the initial ensemble, a grating signal will grow in. This behavior can be qualitatively described by Eq. (2.7) if the exponential decay is replaced with an exponential growth term, so that

$$S(t) = A\, e^{-(\Delta t)^2 k_B T/m}(1 - e^{-kt})^2, \tag{3.1}$$

where k is related to the collision frequency. For very large fringe spacings ($\Delta \to 0$) the Gaussian term becomes a constant, and the signal simply exhibits an exponential buildup. This is the behavior that would be observed in a conventional transient absorption experiment. However, when Δ becomes significant, the Gaussian eventually overwhelms the exponential. Figure 6 illustrates the change in signal [Eq. (3.1)] as a function of the fringe spacing. k has been set equal to the average hard sphere collision frequency at 8.5×10^7 s^{-1}

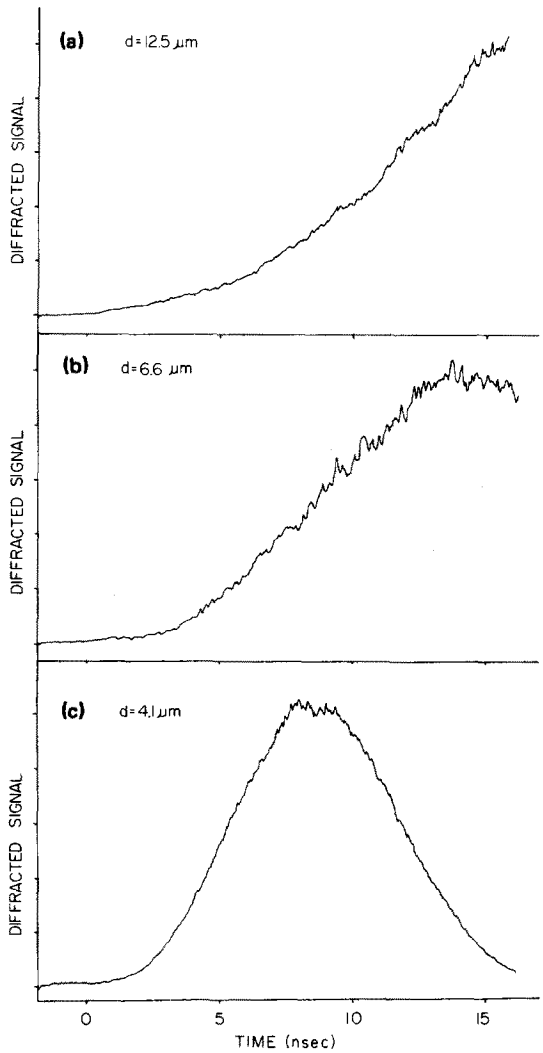

FIG. 5. Fringe spacing dependences of the I_2 grating signal. As the fringe spacing is decreased, the influence of the molecular motion becomes more apparent. The destruction of the grating by molecular motion competes with the collisionally induced buildup of population in the observable state. At smaller fringe spacings molecular motion reduces the grating at earlier times; hence, the signal peaks earlier. The sample temperature and pressure for all three curves are 430 K and 16 Torr.

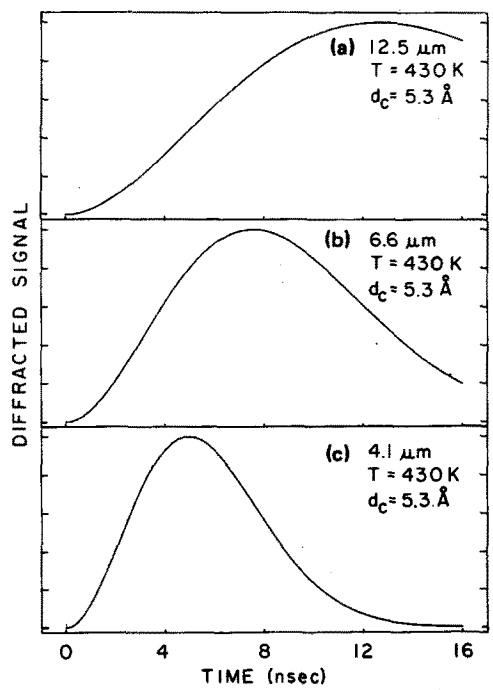

FIG. 6. Curves calculated from the zeroth order model [Eq. (3.1)] for fringe spacings that correspond to the I_2 data shown in Fig. 5. T is the experimentally measured temperature while the collision parameter d_c is an adjustable variable. For this figure d_c has been set equal to the hard sphere collision value of 5.3 Å. The curves behave qualitatively like the data in Fig. 5. With this model, there are no values of d_c that can produce curves which quantitatively agree with data for all the fringe spacings.

($k = \sqrt{2}\pi d_c^2 \langle v \rangle n$; n is the number density which equals 3.6×10^{17} for I_2 at 16 Torr, 430 K). It is clear that Eq. (3.1) is qualitatively in accord with the data in Figs. 4 and 5.

Although Eq. (3.1) is qualitatively correct, it is not an accurate description of the grating data. This zeroth order model does not account for the location of a molecule at the time of collision, nor does it permit the velocities of molecules in the observable ensemble to be different from their velocities in the initial ensemble. Furthermore, in the zeroth order model the velocity dependence of the collision frequency is not included. These deficiencies prevent Eq. (3.1) from providing a quantitative analysis of the data.

To obtain a better understanding of the system dynamics which give rise to the time and fringe spacing dependences of Figs. 4 and 5, a detailed model of the effect of state changing collisions on the grating signal is presented. In this model a single collision takes a molecule from the initial ensemble to the observable ensemble. In a previous publication,[10] calculated curves obtained from a single collision model were presented. The equations from which these were derived were found to be incomplete. As will be shown below, the complete theory presented here provides an accurate description of the data.

B. Theoretical model: Single collision change of state

As mentioned in the previous section, the zeroth order model fails to accurately describe the grating data because it does not allow for changes in velocity of the molecules upon collisions nor does it consider the velocity dependence of the collision frequency. In this section a single collision model that will account for the aforementioned factors is given in detail. The model depicts the situation in which a single collision causes a given excited molecule to change state. The molecule leaves the initial ensemble and enters an observable ensemble. The model keeps track of the trajectory of the molecule by noting where and when the collision takes place and by accounting for initial and final velocities. After a molecule collides once, it is not considered to experience any further collisions. Under these conditions, the time dependence of the spatial profile of the observable ensemble is evaluated.

The single collision model is essentially a convolution problem. The grating results from groups of molecules which scatter at different times. For example, the grating signal at a delay time of 3 ns results from molecules that have undergone state changing collisions at that particular instant and from molecules that have scattered at delay times of 2 ns, 1 ns, etc. In order to calculate the grating signal (for a given fringe spacing d) as a function of time, the time dependent spatial profile of the observable molecules, denoted by N', needs to be considered. Similar to the analysis given in the previous section [see Eqs. (2.2)–(2.5)], the problem involves calculating $N'(y,t)$ at the points $y = 0$ (peaks) and $y = d/2$ (nulls). The grating signal is then taken to be proportional to the square of the peak-null difference in number density $D(t)$. In the following discussion, the appropriate expression for $D(t)$ will be derived in view of the single collision model.

Suppose a molecule with an initial velocity v is excited at time $t = 0$. If the molecule collides at time t' (thereby entering the observable ensemble) and acquires a new velocity v', then the total distance traveled by the molecule along the grating wave vector (y direction) at the observation time t is

$$\delta y = v_y t' + v_y'(t - t') . \tag{3.2}$$

The relative concentration of observable molecules that appear at position y at time t, which have collided at time t' and have had a velocity change of $v \to v'$, is

$$N'(y,t,t',v,v') = \tfrac{1}{2}(\cos\{\Delta[y - v_y t' - v_y'(t - t')]\} + 1) \times P(v \to v')P(t',v) . \tag{3.3}$$

In comparison to the expression in Eq. (2.3), the argument of the cosine reflects the total distance traveled by the molecules. The term $P(v \to v')$ describes the probability that a molecule starts with an initial velocity v and ends up with a final velocity v' after a collision. $P(t',v)$ is the probability per unit time that a molecule with velocity v will undergo a collision at time t'. The total number of observable molecules arriving at position y at time t, $N'(y,t)$, is obtained by integrating Eq. (3.3) over the velocities v and v' and over the scattering time t':

$$N'(y,t) = \int_v \int_{v'} \int_{t'} \frac{1}{2}(\cos\{\Delta[y - v_y t' - v_y'(t - t')]\} + 1) \times P(v \to v')P(t',v)\,dt'\,dv'\,dv . \tag{3.4}$$

The peak-null difference in the concentration of molecules in the observable state is derived from Eq. (3.4):

$$D(t) = N'(0,t) - N'(d/2,t) \tag{3.5a}$$

$$= \int_v \int_{v'} \int_{t'} \cos\Delta[v_y t' + v_y'(t - t')] \times P(v \to v')P(t',v)\,dt'\,dv'\,dv . \tag{3.5b}$$

Equation (3.5b) is a general expression for the single collision model since the two probability terms have not yet been specified. In order to perform the above integration, one must first define $P(t',v)$. If the relative population of N' molecules with velocity v, $N'(t,v)$, exhibits an exponential buildup of the form $1 - e^{-k_v t}$, where k_v is a velocity dependent collision frequency, then

$$N'(t,v) = \int_0^t P(t',v)\,dt' = 1 - e^{-k_v t} \tag{3.6a}$$

and

$$P(t',v) = \left(\frac{\partial N'(t',v)}{\partial t'}\right)_v = k_v\, e^{-k_v t'} . \tag{3.6b}$$

Substitution of the above expression for $P(t',v)$ in Eq. (3.5b) yields

$$D(t) = \int_v \int_{v'} \int_{t'=0}^{t} k_v\, e^{-k_v t'} P(v \to v') \times \cos\Delta[v_y t' + v_y'(t - t')]\,dt'\,dv'\,dv . \tag{3.7}$$

Equation (3.7) is still a general expression since the scattering probability function $P(v \to v')$ has not been defined. As mentioned earlier, $P(v \to v')$ gives the probability

that a molecule with an initial velocity v scatters into a final velocity v'. Two limits for $P(v \rightarrow v')$ will be considered. In the first case (model I), the state changing collision does not change the molecular velocity. Thus a molecule that scatters into the observable ensemble continues to move with its initial velocity. This model preserves the molecular trajectories and the translational temperature of the initial ensemble. In model II, the velocity of a molecule is randomized by the state changing collision. The final velocity distribution is Maxwell–Boltzmann with a temperature T_f that is not necessarily equal to the initial temperature T.

$P(v \rightarrow v')$ for the two limiting models is given by

model I:

$$P(v \rightarrow v') = e^{-mv^2/2k_BT}\delta_{v,v'} ; \tag{3.8}$$

model II:

$$P(v \rightarrow v') = e^{-mv^2/2k_BT} \times e^{-mv'^2/2k_BT_f} . \tag{3.9}$$

Both models I and II result in observable ensemble velocity distributions which are Maxwell–Boltzmann distributions with well defined temperature. It is possible, that following state changing collisions, the velocity distribution is not Gaussian with a definite temperature. This point will be discussed following the data analysis.

First consider model I. Substituting Eq. (3.8) into Eq. (3.7) gives

$$D(t) = \int_v \int_{t'=0}^{t} k_v \, e^{-gv^2} \cos(\Delta v_y t) e^{-k_v t'} \, dt' \, dv , \tag{3.10}$$

where $g \equiv m/2k_BT$. Integrating over time yields

$$D(t) = \int_v e^{-gv^2} \cos(\Delta v_y t)(1 - e^{-k_v t}) \, dv . \tag{3.11}$$

The velocity dependent collision rate k_v is given by

$$k_v = s(v_x^2 + v_y^2 + v_z^2 + \langle v \rangle^2)^{1/2} , \tag{3.12a}$$

where

$$s = \pi d_c^2 n . \tag{3.12b}$$

If k_v in Eq. (3.11) is replaced by an average collision frequency $\bar{k}$ ($\bar{k} = \sqrt{2}\,\pi d_c^2 \langle v \rangle n$), then the subsequent integration over the velocity gives the peak-null difference for the zeroth order model discussed earlier [see Eq. (3.1)]. The zeroth order model describes the case in which the initial ensemble simply damps into the observable ensemble. As mentioned previously, the zeroth order model does not accurately describe the data.

The full analysis of model I involves the integration of Eq. (3.11), which cannot be done analytically. However, the integration can be reduced to a two-dimensional problem by noting the symmetry between v_x and v_z. If a change to a cylindrical coordinate system is made by defining $v_x^2 + v_z^2 \equiv v_1^2$ and $dv_x \, dv_z \equiv v_1 dv_1 \, d\phi$, integration over the azimuthal angle in velocity space can be performed. Substituting Eq. (3.12) into Eq. (3.11), carrying out the tranformation, and integrating over ϕ yields

$$D(t) = 2\pi \int_{v_y} \int_{v_1} v_1 \, e^{-g(v_y^2 + v_1^2)} \times \cos(\Delta v_y t)\left(1 - e^{-s(v_y^2 + v_1^2 + \langle v \rangle^2)^{1/2} t}\right) dv_1 \, dv_y . \tag{3.13}$$

Equation (3.13) was integrated numerically using the Gaussian quadrature method. The results for a fringe spacing of 4.1 μm, a temperature of 430 K (the sample temperature) and two collision parameters are compared to the data in Fig. 7. Note that as the collision parameter is increased the maximum shifts to earlier time. The maximum of the calculated curve will not coincide with the data for any choice of the collision parameter. For a collision parameter of 5.3 Å or less, the maximum always occurs at approximately 4.5 ns. It is clear from the figure that model I does not accurately describe the data. Similar results were obtained for different fringe spacings. The fact that model I does not allow for velocity changing collisions results in the model's inability to reproduce the experimental grating curves.

For model II, Eq. (3.9) is used for $P(v \rightarrow v')$ in Eq. (3.7). The equation for the peak-null difference becomes

$$D(t) = \int_v \int_{v'} \int_{t'=0}^{t} k_v \, e^{-gv^2} e^{-g'v'^2} \times \cos \Delta\left[v_y t' + v_y'(t - t')\right] e^{-k_v t'} \, dt' \, dv' \, dv . \tag{3.14}$$

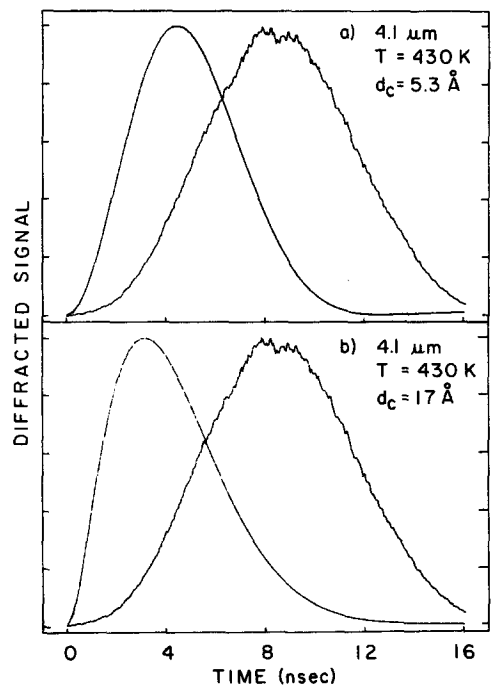

FIG. 7. Comparison of I_2 data obtained at 4.1 μm with curves calculated from model I [Eq. (3.13)]. In this model the velocity of a molecule is unchanged by the state changing collision and the temperature T is the sample temperature. d_c is an adjustable parameter which is given values of 5.3 and 17 Å in parts (a) and (b), respectively. Note that an increase in the collision parameter d_c shifts the maximum to earlier times. For $d_c \lesssim 5.3$ Å, the maximum occurs at roughly 4.5 ns. Consequently, model I cannot be made to fit the data and is, therefore, not an accurate description of the I_2 system.

Integrating over t' and combining various terms yields

$$D(t) = \int_v \int_{v'} \frac{k_v\, e^{-gv^2} e^{-g'v'^2}}{k_v^2 + \Delta^2(v_y' - v_y)^2} \times [k_v \cos(\Delta v_y' t) + \Delta(v_y' - v_y)\sin(\Delta v_y' t) - e^{-k_v t}\Delta(v_y' - v_y)\sin(\Delta v_y t) - e^{-k_v t} k_v \cos(\Delta v_y t)]\, dv'\, dv . \quad (3.15)$$

Equation (3.15) can be somewhat simplified by eliminating the integration over v_x' and v_z' since these variables do not affect the time dependence:

$$D(t) = \int_v \int_{v_y'} \frac{k_v\, e^{-gv^2 - g'v_y'^2}}{k_v^2 + \Delta^2(v_y' - v_y)^2} \times \{k_v \cos(\Delta v_y' t) + \Delta(v_y' - v_y)\sin(\Delta v_y' t) - e^{-k_v t'}[k_v \cos(\Delta v_y t) + \Delta(v_y' - v_y)\sin(\Delta v_y t)]\}\, dv_y'\, dv . \quad (3.16)$$

To further reduce the dimensionality of the problem, one can perform the transformation to cylindrical coordinates [see Eq. (3.13)] for the unprimed velocity components and integrate over the azimuthal angle. The time dependence of the peak-null difference from Eq. (3.16) becomes

$$D(t) = 2\pi s \int_{v_y} \int_{v_y'} \int_{v_1} \frac{e^{-g(v_y^2 + v_1^2) - g'v_y'^2}}{s^2(v_y^2 + v_1^2 + \langle v\rangle^2) + \Delta^2(v_y' - v_y)^2} (v_y^2 + v_1^2 + \langle v\rangle^2)^{1/2} v_1 \times [s(v_y^2 + v_1^2 + \langle v\rangle^2)^{1/2} \cos(\Delta v_y' t) + \Delta(v_y' - v_y)\sin(\Delta v_y' t) - e^{-s(v_y^2 + v_1^2 + \langle v\rangle^2)^{1/2} t}[s(v_y^2 + v_1^2 + \langle v\rangle^2)^{1/2} \cos(\Delta v_y t) + \Delta(v_y' - v_y)\sin(\Delta v_y t)]]\, dv_1\, dv_y'\, dv_y . \quad (3.17)$$

In the above equation, the explicit expression for k_v [Eq. (3.12)] has been employed.

Integration of Eq. (3.17) was performed using the Gaussian quadrature method for the v_y and v_y' variables and Simpson's rule for the v_1 coordinate. Typically, the range of integration required for convergence was from 0 to $\pm 5\times 10^4$ cm/s. The two adjustable parameters for this model are the collision parameter d_c ($s = \pi d_c^2 n$) and the final temperature T_f ($g' = m/2k_B T_f$). In Tables I and II, the results for a one parameter and two parameter fit are listed for several fringe spacings. In the one parameter fit, the final temperature T_f was set equal to the initial temperature of 430 K and d_c was allowed to vary. For the two parameter case both the final temperature and d_c were allowed to vary. Figures 8(a)–8(e) compare the data to curves generated from Eq. (3.17) using the parameters listed in Table II. (Curves drawn using the Table I parameters give essentially the same results.) The theoretical curves in Fig. 8 show good agreement with the data. The overall results demonstrate that the model is an essentially accurate description of the collisional process. The temperature in Table II are all close to the ambient temperature of 430 K. Although the cross sections vary from curve to curve, they lie within a narrow range. The average value of the collision parameter for the change of state is 3.8 Å, which is significantly smaller than the hard sphere collision parameter of 5.3 Å.

Some cross sections for various energy transfer processes involving iodine collisions with iodine as well as with other molecules have been studied. An extensive review of the experimental results for I_2 is given by Steinfeld.[21] Cross sections for quenching the B state of iodine (where the collision partner is a ground state molecule) listed by Steinfeld are on the order of 200 Å^2. For vibrational energy transfer within the B manifold, total cross sections are given as 88 and 19 Å^2 for $v = 15$, $j = 33$ and $v = 43$, $j = 12, 16$, respectively. In comparison, the average cross section obtained from Table II, 45 Å^2, is certainly reasonable.

Although model II is in good agreement with the data, it is not perfect, since a small range of cross sections is obtained. This range could be the result of physical factors that are not taken into account by the model. First, only the effect of the single collision which causes the change to the observable state is considered. Secondary collisions, which may or may not cause state changes, can certainly alter the velocity. The single collision model which does not account for these secondary collisions uses an effective cross section to describe both the change of state and the velocity change. The model yields a value of the cross section which is smaller than hard sphere. It is, therefore, not unreasonable to assume that by the time a state changing collision occurs, the velocity has been somewhat but not completely randomized. The choice of the velocity scattering probability is another

TABLE I. Model II: One parameter fit (d_c).

$d(\mu m)$	d_c(Å)	σ(Å^2)	T_f(K)
12.5	3.3	34	430
6.6	3.3	34	430
5.5	3.1	30	430
4.6	4.4	61	430
4.1	4.9	75	430

TABLE II. Model II: Two parameter fit (d_c,T_f).

$d(\mu m)$	d_c(Å)	σ(Å^2)	T_f(K)
12.5	3.4	36	405
6.6	3.3	34	420
5.5	3.1	30	420
4.6	4.4	61	425
4.1	4.5	64	480

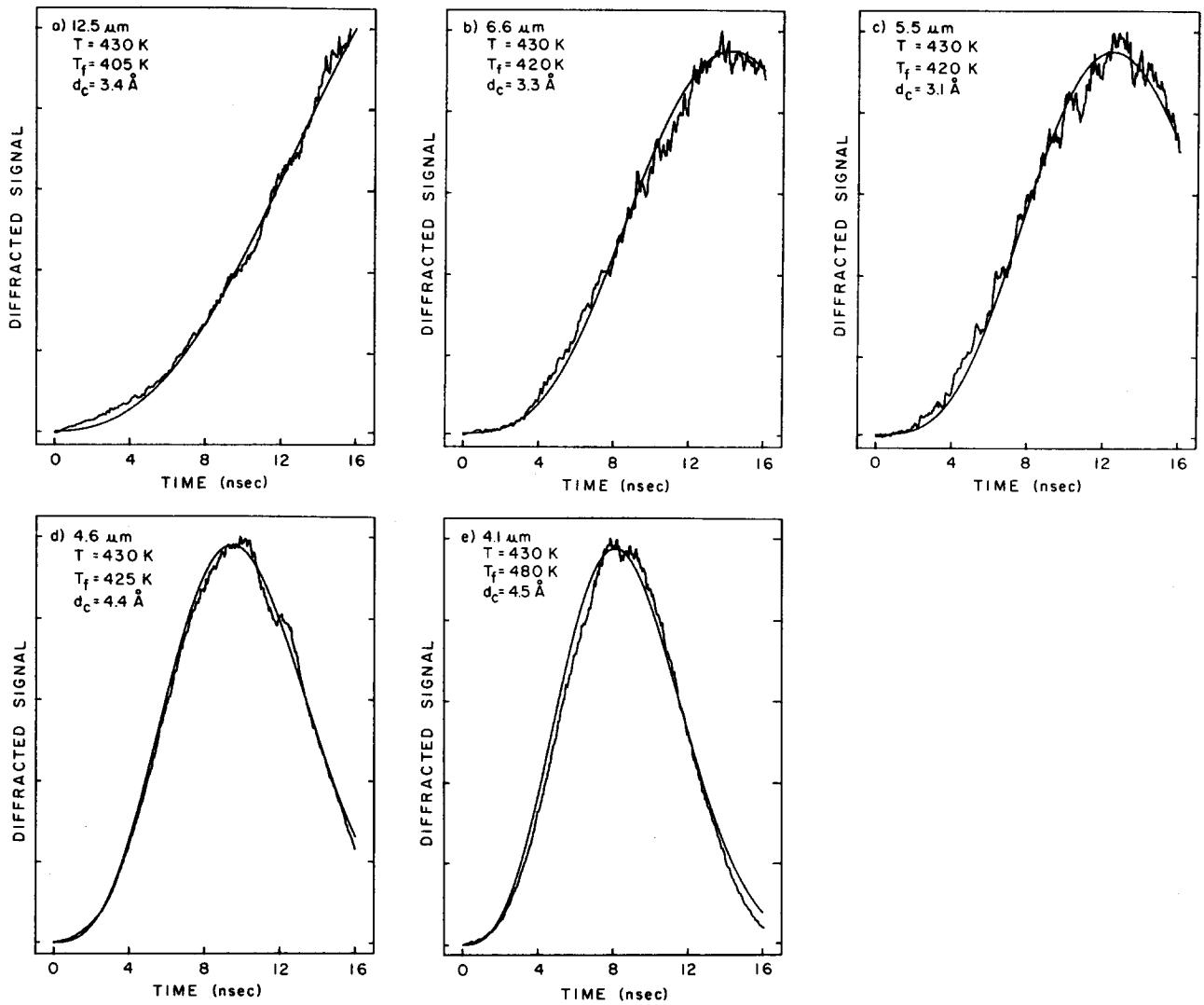

FIG. 8. Comparison of model II [Eq. (3.17)] curves generated from the best fit parameters (listed in Table II) with I_2 data taken at five different fringe spacings. In this model the velocity of each molecule is randomized upon collision. The initial velocity distribution is characterized by an initial temperature which is set equal to the measured sample temperature T. The final velocity distribution is characterized by T_f which is an adjustable parameter. The second adjustable parameter in the model is d_c, the collision parameter. These results demonstrate that model II is an accurate description of the collision dynamics.

point. The probability employed in model II not only randomizes the velocity, but assumes that the final distribution is governed by a well-defined temperature. This form of the scattering function would not be appropriate for a non-Boltzmann final velocity distribution. An improvement over the single collision model would involve the use of two distinct cross sections: one for the state changing collision and another for velocity changing collisions. The latter cross section would describe the decay of the velocity autocorrelation function. An additional consideration that has been neglected in the single collision model is the fact that the grating signal may not result from a single state. If many states are involved there could be several distinct cross sections.

In the I_2 experiments, the identity of the state or states giving rise to the strong absorption at 532 nm, and hence the grating diffraction, is at present unknown. The strong signal indicates that the probe transition must be spin allowed. Furthermore, the buildup of signal with time demonstrates that the origin of the transition must be a bound state. However, the final state produced by interaction of the observable ensemble with the probe need not be bound. (The grating is not affected by events which occur after the probe has interacted with the sample.) From the I_2 energy level diagram given by Mulliken[22] and the wavelengths of the probe and excitation pulses, it seems reasonable to propose that the grating signal can be attributed to transitions from either one of the bound $A(^3\Sigma_{1u}, ^3\Sigma_{2u})$ states to one of the unbound states from the 2422 family $(^3\Sigma^-_{g(1)}, ^3\Sigma_{g(0^+)})$. Another possibility would be for the transition to occur from an excited vibrational level of the ground state manifold $(^1\Sigma_g^+)$ to the dissociative $^1\Pi_u$ state of the 2431 family. An attempt to locate the origin of the transition was made by tuning the excitation wavelength between 560 and 670 nm. The signal became weaker as the wavelength was tuned to the red of 560 nm and disappeared altogether at 630 nm. The shape of the grating decays remained constant and a signal at $t = 0$ was never observed. The identification of this 532 nm transition is open for further investigation.

IV. ULTRAHIGH RESOLUTION POLARIZATION GRATING SPECTROSCOPY: Na EXPERIMENTS AND THEORY

A normal population grating is established by the interference of two crossed excitation pulses which have the same polarization. If the polarization of one of the excitation pulses is rotated by 90°, a polarization grating is generated (see Fig. 1). In a population grating, the two excitation pulses constructively and destructively interfere to produce the optical fringe pattern. The interference results from the changing phase relationship of the two overlapping beams along the grating axis (y direction in Fig. 1). When the two pulses have perpendicular polarizations they cannot interfere. However, the two fields will add vectorially. If one pulse is polarized vertically (along x) and the other horizontally (along y), then when their relative phase is 0 [see Fig. 1(c)] the E fields will add to give linearly polarized light with a polarization that bisects the vertical and horizontal axes [left-hand side of Fig. 1(c)]. As one moves to the right along the grating axis y, the two pulses are no longer in phase. This results in elliptically polarized light. When the phase difference is $\pi/2$, the light is circularly polarized [left circular polarized (lcp) in Fig. 1(c)]. Moving further to the right gives elliptically polarized and then linearly polarized light at a relative phase of π. The linearly polarized light at π is perpendicular to the linearly polarized light at 0. Moving from 0 to π corresponds to one-half a fringe in a normal parallel grating. Continuing to the right the field again becomes elliptical and at $3\pi/2$ it is now right circular polarized (rcp). Finally at 2π, the field is again linearly polarized. Zero to 2π corresponds to one complete fringe in a parallel grating. While the polarization varies from linear to circular for perpendicularly polarized excitation pulses, the total intensity (the square of the absolute value of the electric field) is constant everywhere.

A comparison between Na population and polarization grating decays for a fringe spacing of 12.2 μm is shown in Fig. 9. The polarization grating data [Fig. 9(b)] was taken with the excitation beams tuned to the $^2P_{1/2}$ manifold and the linearly polarized probe tuned to the $^2P_{3/2}$ manifold. The interchange of the probe and excitation wavelengths does not effect the population grating signal, but it does effect the polarization grating as discussed below. The temperature and fringe spacing are the same for both scans. The polarization grating signal, which is linearly polarized and rotated 90° with respect to the probe, exhibits pronounced oscillations which are independent of the fringe spacing. The oscillation frequency is identical to the Na ground state hyperfine splitting of 1.77 GHz.[23] The overall envelope of the signal maintains the Gaussian shape exhibited by the population grating signal. Both scans contain a coherence spike at short times.

When the excitation and probe pulses are tuned into the same spin-orbit manifold the pattern of oscillations is different (see Fig. 10). In Fig. 10, both the excitation and probe are resonant with the $^2P_{1/2}$ manifold. (The temperature is approximately the same as in Fig. 9 and the fringe spacing is again 12.2 μm.) Unlike the two color result, the polarization grating signal envelope does not appear to match the popula-

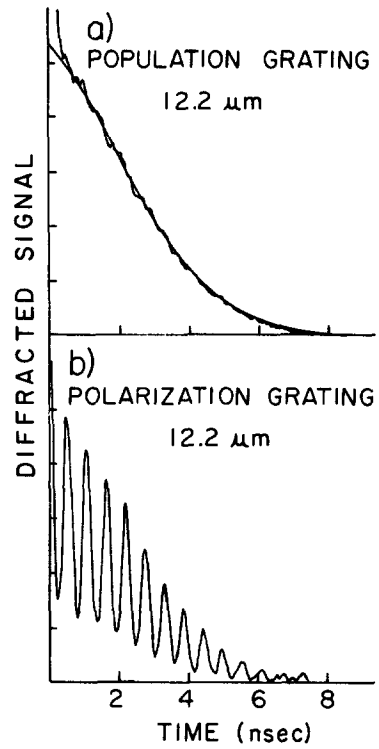

FIG. 9. (a) Population grating. Fringe spacing = 12.2 μm; λ_{exc} = 589.0 nm; λ_p = 589.6 nm; T = 585 K. The solid line through the data is the theoretical fit (T_f = 590 K). (b) Polarization grating. Fringe spacing = 12.2 μm; λ_{exc} = 589.6 nm; λ_p = 589.0 nm; T = 605 K. The observed oscillations in the polarization grating data correspond to the ground state hyperfine splitting of 1.77 GHz. The polarization grating signal envelope follows that of the population grating when the probe and excitations are tuned into different excited state manifolds. The interchange of the probe and excitation wavelength does not affect the population grating signal.

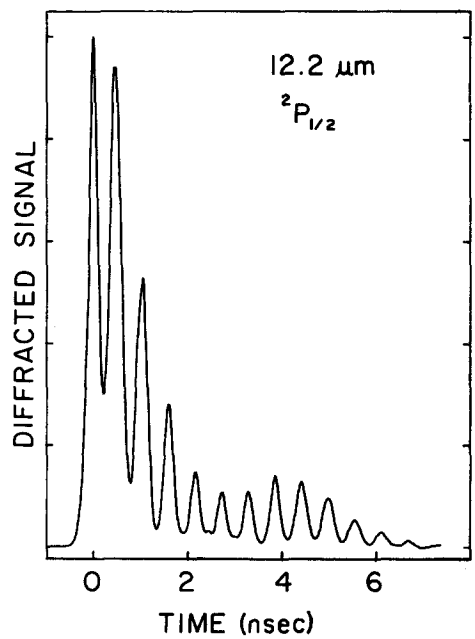

FIG. 10. Na polarization grating. Both the probe and excitation pulses are tuned into the $^2P_{1/2}$ manifold. The high frequency oscillations result from $^2S_{1/2}$ ground state hyperfine splitting (1.77 GHz). A slower oscillation, which results in a peak at ~4 ns, is due to the excited state hyperfine interaction (189 MHz). The oscillation from the excited hyperfine states is shifted by the Gaussian envelope decay to earlier time. (Fringe spacing = 12.2 μm; T = 585 K.)

tion grating decay curve. This is because there is an additional low frequency component in the oscillation. A single maximum for this component is observed at $t \cong 4$ ns. This second component is a manifestation of the excited state ($^2P_{1/2}$) hyperfine splitting of 189 MHz. The maximum is shifted somewhat to shorter time (4 ns as opposed to 5.3 ns) because of the damping from the Gaussian envelope. In Fig. 11, the probe and excitations are tuned into the $^2P_{3/2}$ manifold. While still clearly visible, the oscillations are significantly smaller than for the $^2P_{1/2}$ case. The scan in Fig. 12 was taken with the sodium cell placed in a static magnetic field of ~900 G. The magnetic field splits the degenerate sodium hyperfine levels giving rise to additional frequency components. The magnetic field effect further demonstrates that the oscillations are the result of the hyperfine structure of the sodium atom.

Figure 13 is a schematic illustration of the Na energy level structure taken from Rothberg and Bloembergen.[23] The ground state has an unpaired electron in the $3S$ orbital. In the excited state, the unpaired electron occupies the $3P$ orbital. The spin-orbit interaction couples the electron spin s with the orbital angular momentum l to give rise to the spin-orbit states with angular momenta J. In the ground state $l = 0$ so that $s = J = 1/2$, while in the excited state $l = 1$, giving $J = 3/2$ and $J = 1/2$. However, the Na nuclear spin, $I = 3/2$. For the ground state, the Fermi contact hyperfine interaction couples I and s to give the states $F = I + J = 2$ and $F = I - J = 1$. Associated with each F are the $2F + 1$, M_F, magnetic substates. In the absence of a magnetic field the M_F states are degenerate. Therefore, the state $F = 2$ is fivefold degenerate while $F = 1$ is threefold degenerate. For

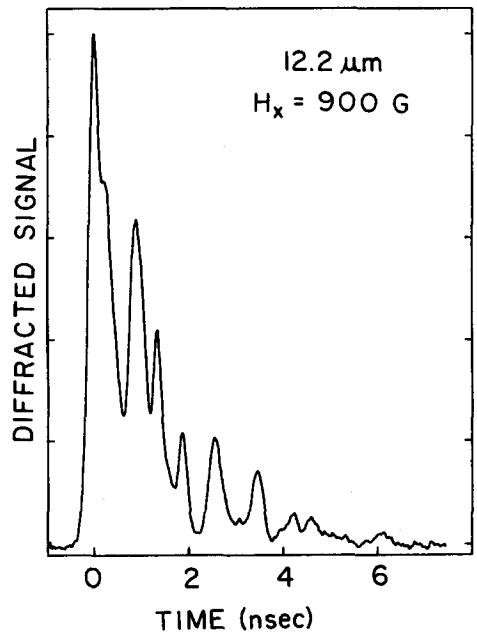

FIG. 12. The experimental conditions are the same as those described in Fig. 10 except that a static magnetic field of ~900 G is applied in the x direction. The magnetic field splits the degeneracy of the $|FM_F\rangle$ hyperfine states causing additional frequency components to occur in the grating decay.

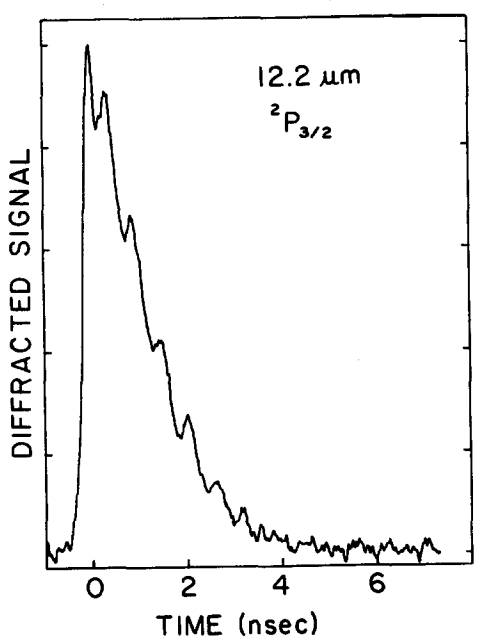

FIG. 11. Na polarization grating signal obtained when the probe and excitation pulses are tuned into the $^2P_{3/2}$ manifold. The ground state modulations are much less pronounced in this situation than for the $^2P_{1/2}$ case shown in Fig. 10. The effect of the excited state splittings on the signal envelope, however, is comparable for both manifolds. (Fringe spacing = 12.2 μm; T = 585 K.)

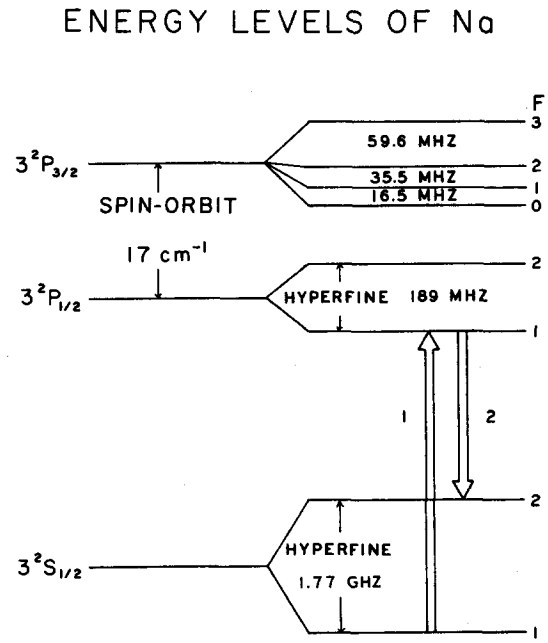

FIG. 13. Energy level diagram of the Na atom. The hyperfine interaction splits the ground state into two levels which are separated by 1.77 GHz. The excited state is split into two manifolds by spin-orbit coupling. These two manifolds are further split into various hyperfine levels. The hyperfine levels for both the S and P manifolds are characterized by the combined nuclear and electronic angular momentum quantum number F. Each F level is a multiplet of $2F + 1$ degenerate states. In the presence of a magnetic field, the states within the multiplets are no longer degenerate, but are separated by the Zeeman splitting. The double arrows represent one possible pathway for multiple interactions with the radiation field.

the excited states, the Fermi contact interaction is zero. However, the anisotropic hyperfine interaction[24] couples $J = 1/2$ with $I = 3/2$, to give two values of F, 2 and 1 and $J = 3/2$ with $I = 3/2$ to give rise to four F values, 3, 2, 1, and 0. Again each F value has associated with it $2F + 1$ M_F states which are degenerate in the absence of a magnetic field.

The hyperfine oscillations in the polarization grating arise from the interplay of three factors. (1) Optical transitions between ground and excited state hyperfine levels obey $\Delta M_F = \pm 1$ selection rules. In the coordinate convention that is employed in this discussion, $\Delta M_F = +1$ transitions are induced by rcp light and $\Delta M_F = -1$ transitions are induced by lcp light. (2) The polarization grating excitation contains spatial regions which are rcp and regions which are lcp (see Fig. 1). (3) The picosecond pulses are of sufficiently high intensity that the Rabi frequency spans all levels in the ground state hyperfine manifold and in the excited state manifold. Therefore, any transition which is permitted by the selection rules can be driven by the laser fields.

Previously, polarization gratings have been analyzed for systems of randomly oriented molecules with well-defined transition dipole moments[25] or in terms of a Kerr effect.[26] In those experiments, the probe is resolved into two linear vectors $\hat{e}_1$ and $\hat{e}_2$ shown in Fig. 1(c). For an absorption polarization grating, the regions that are oriented along $\hat{e}_1$ exhibit partial bleaching in that direction. The sample absorbs the $\hat{e}_2$ component of the probe more strongly than the $\hat{e}_1$ component. The opposite response occurs for the grating region oriented along $\hat{e}_2$. The circular regions of the grating absorb the $\hat{e}_1$ and $\hat{e}_2$ components of the probe equally. The net result is that the two components of the probe experience two distinct gratings which are spatially shifted from each other along the grating wave vector by half a grating wavelength. Because of this spatial shift, the outgoing $\bar{E}$ fields from the two gratings are phase shifted by exactly 180°. This results in a rotation of the signal polarization by 90° with respect to a probe polarized parallel to one of the excitation polarizations.

For the sodium excited state polarization grating, the vectorial analysis discussed above cannot explain the grating diffraction since an atom does not have an intrinsic direction for the transition dipole. However, if one decomposes the probe into right and left circularly polarized components, one can show that the rcp and lcp excited regions of the grating behave differently. This results from the $\Delta M_F = +1$ or -1 selection rule for rcp or lcp light. (The convention that is used in this discussion is as follows: rcp light exhibits clockwise rotation in a right-handed coordinate system when observed along the propagation axis, namely the positive z axis. The selection rule $\Delta M_F = -1$ for lcp and $\Delta M_F = +1$ for rcp, is consistent with this convention.) In the regions excited by rcp light, $\Delta M_F = +1$ transitions are partially bleached. Correspondingly, in the regions excited by lcp light, $\Delta M_F = -1$ transitions are partially bleached. The rcp and lcp excited regions of the grating interact differently with the right and left components of the probe. In contrast, the linear parts of the grating are excited by both circular polarizations, and therefore, interact identically with both probe components. Consequently, the two components of the probe experience two distinct gratings, spatially shifted by a half grating wavelength. This results in the observed 90° rotation of the signal polarization relative to the probe polarization.

The modulations in the signal intensity only appear in the polarization grating. These modulations, which persist well beyond the free induction decay time associated with the Doppler linewidth, cannot result from a macroscopic polarization beating. Furthermore, the number density is sufficiently low to preclude multiatom quantum beat effects. Hence, the modulations must arise from a single atom phenomenon. The oscillation in signal amplitude results from coherent superposition states formed on each atom by the excitation pulses. Because the oscillator strengths of the $^2S_{1/2}$ to $^2P_{3/2,1/2}$ transitions are large,[27] multiple interactions with the excitation field occur readily. The Rabi angle for a 100 nJ, 18 ps excitation pulse focused to a spot size of 200 μm is approximately 7 π. Thus, state from both ^2S hyperfine levels will be coupled via transitions to and from the ^2P manifold. Since the Rabi frequency is much larger than the hyperfine splitting, couplings between all the hyperfine states are energetically possible.

Figure 13 displays one possible multiple interaction with the field. The double arrows indicate field induced couplings between the ground and excited state. A state from the $^2S_{1/2}$, $F = 1$ manifold is coupled to a state from the $^2P_{1/2}$, $F = 1$ manifold with the appropriate change of M_F, e.g., for a rcp field, $\Delta M_F = +1$. This process is indicated by the arrow labeled 1. The field couples the resulting excited state to a state of the ground level $F = 2$ manifold, again with a change of M_F. This is indicated by an arrow labeled 2. The result in this example is the production of a three ket superposition state involving kets from both ground state hyperfine manifolds. The kets in the superposition have time dependent phase factors which have frequency differences at the hyperfine splitting. As will be shown in detail below, the phase factors result in a time dependent transition probability which oscillates at the hyperfine splitting. The oscillating transition probability gives rise to an oscillating diffraction efficiency which results in the modulations of the observed signal.

Recently there has been considerable interest in the nonlinear optical properties of sodium vapor. Four wave mixing (FWM) experiments have been performed in the frequency domain to obtain information concerning the third order susceptibility $\chi^{(3)}$ [28–32] and the effects of collisions with buffer gases.[23] Time domain FWM experiments such as the trilevel echo,[33] two-photon echo,[34] stimulated echo,[35] grating echo,[36] and backward photon echo[37] have also been employed to study collisional relaxation as well as investigate the effects of pulsed incoherent light.[38]

Unlike fluorescence quantum beat experiments,[39,40] nonlinear experiments, such as FWM, involve higher order interactions with the E fields which can reveal ground state splittings. In these nonlinear experiments, a macroscopic polarization is generated which will exhibit the beat frequency.[41] A transient grating experiment is inherently different from typical time-delayed four-wave mixing experiments in

that the grating does not require the interaction of a probe pulse with a macroscopic polarization. The intensity of the grating signal pulse is given by the grating diffraction efficiency which is a function of the peak-null difference in the refractive index. (At probe delay times less than the free induction decay period a macroscopic polarization exists in the sample. The macroscopic polarization gives rise to the coherence spike in the grating decay curve.)

In the normal grating framework, it is not obvious how a hyperfine oscillation might be observed. The transient grating signal is the portion of the probe induced free-induction decay that constructively interferes in the Bragg diffraction direction to give rise to the signal.[42] The magnitude of the diffraction for an excited state grating is determined by the peak-null difference in the excited state number density.[8,42] Therefore, the modulations in the grating signal can only result from modulations in the diffraction efficiency.

To obtain a detailed understanding of the Na polarization phenomena, it is necessary to address the problem quantitatively. It is particularly important to explain the appearance of hyperfine oscillations in the polarization grating data and the absence of oscillations in the population grating data. The qualitative discussion presented in connection with Fig. 13 does not reveal the major difference between the two types of experiments. It is also necessary to understand why the modulations are less pronounced in the $^2P_{3/2}$ data (Fig. 11) than in the $^2P_{1/2}$ data (Fig. 9), and why the two color polarizating grating data (Fig. 9) exhibits only the ground state hyperfine frequency while the one color data (Fig. 10) exhibits both ground and excited state hyperfine frequencies.

The exact solution of the grating problem involves treating a multilevel system coupled to both linear and circularly polarized light. In principle, analytical solutions for certain multilevel problems can be obtained if a multilevel rotating wave approximation (RWA) can be applied.[43] However, the difficulty of the solution increases dramatically as the number of levels increases. Furthermore, for the situation in which the transitions are driven by rcp and lcp circularly polarized light, as they are in sodium, the treatment of an interaction with a linear field cannot employ the RWA.

The ground state ($^2S_{1/2}$) has eight hyperfine levels as does the $^2P_{1/2}$ state. Therefore, an analysis involving these electronic manifolds involves 16 states. A detailed, quantitative understanding of the problem can be obtained by limiting the consideration to four states. If the system is taken to be in a particular ground eigenket, only certain states can be coupled to the initial eigenket through multiple interactions with the field. Because of the $\Delta M_F = \pm 1$ selection rules, not all states are involved when a particular initial state is chosen. The following derivation of the grating diffraction efficiency from a limited set of states will illustrate the principal features of the experiments. Extensions to a full treatment are discussed following the development.

In a polarization grating, the regions excited by lcp light are subject to the selection rule $\Delta M_F = -1$. If the initial ground state is $|10\rangle_S$, the following superposition can be formed by the interaction with the lcp field[44]:

$$|\psi_L\rangle = a|10\rangle_S\, e^{-i\omega_1 t} + b\,|1\,-1\rangle_P\, e^{-i\omega_2 t} + c|20\rangle_S\, e^{-i\omega_3 t} + 0|11\rangle_P\, e^{-i\omega_2 t}. \tag{4.1}$$

The subscripts on the kets indicate whether they belong to the ground state (S) or the excited state (P). (Note that even though the $|11\rangle$ state is not excited, its inclusion in the superposition state with a zero coefficient is necessary for the subsequent analysis.) In the rcp regions, a different superposition state is formed:

$$|\psi_R\rangle = a'|10\rangle_S\, e^{-i\omega_1 t} + b'|11\rangle_P e^{-i\omega_2 t} + c'|20\rangle_S\, e^{-i\omega_3 t} + 0|1\,-1\rangle_P\, e^{-i\omega_2 t}. \tag{4.2}$$

The states $|\psi_R\rangle$ and $|\psi_L\rangle$ given in Eqs. (4.1) and (4.2) are generated during the time the excitation pulses are in the medium. Once, the pulses have left the sample, the coefficients a, a', b, b', c, and c', in the absence of fluorescence, remain constant in time.

As mentioned earlier, the oscillations in the polarizations grating signal result from time dependence oscillations in the grating diffraction efficiency. To calculate the time dependent diffraction efficiency it is necessary to analyze the interaction between the field and the atomic system in terms of the uncoupled atomic basis states $|m_I m_l m_s\rangle$, where I, l, and s are the nuclear, orbital, and spin angular momenta. The supersposition state $|\psi_L\rangle$ [Eq. (4.1)] can be written in terms of the uncoupled basis states (see the Appendix):

$$\begin{aligned}|\psi_L\rangle = \sqrt{2}\,M\Big[&\cos\frac{\Delta\omega t}{2}|-1/2\ \ 0\ \ 1/2\rangle_S - i\sin\frac{\Delta\omega t}{2}|1/2\ \ 0\ \ -1/2\rangle_S\Big]\, e^{-i\Omega t}\\ &+ b\Big[\frac{1}{\sqrt{2}}|-3/2\ \ 1\ \ -1/2\rangle_P - \frac{1}{2}|-3/2\ \ 0\ \ -1/2\rangle_P - \frac{1}{2\sqrt{3}}|-1/2\ \ 0\ \ -1/2\rangle_P\\ &+ \frac{1}{\sqrt{6}}|-1/2\ \ -1\ \ 1/2\rangle_P\Big]\, e^{-i\omega_2 t} + 0\Big[\frac{1}{\sqrt{2}}|3/2\ \ -1\ \ 1/2\rangle_P - \frac{1}{2}|3/2\ \ 0\ \ -1/2\rangle_P - \frac{1}{2\sqrt{3}}|1/2\ \ 0\ \ 1/2\rangle_P\\ &+ \frac{1}{\sqrt{6}}|1/2\ \ 1\ \ -1/2\rangle_P\Big]\, e^{-i\omega_2 t} + |S_L\rangle\,. \end{aligned}\tag{4.3}$$

In Eq. (4.3), the hyperfine frequency $\Delta\omega = (\omega_3 - \omega_1)$, the average frequency $\Omega = (\omega_1 + \omega_3)/2$, $M = (a + c - |a - c|)/2$ (this is the modulation depth factor), and $|S_L\rangle$ represents an additional term which occurs if $a \neq c$. Note that M essentially gives the smaller value of the coefficients a and c.

In an analogous manner the rcp superposition state [Eq. (4.2)] can be written as

$$|\psi_R\rangle = \sqrt{2}\,M'\left[\cos\frac{\Delta\omega t}{2}|-1/2\ 0\ 1/2\rangle_S - i\sin\frac{\Delta\omega t}{2}|1/2\ 0\ -1/2\rangle_S\right]e^{-i\Omega t}$$
$$+ b'\left[\frac{1}{\sqrt{2}}|3/2\ -1\ 1/2\rangle_P - \frac{1}{2}|3/2\ 0\ -1/2\rangle_P - \frac{1}{2\sqrt{3}}|1/2\ 0\ 1/2\rangle_P\right.$$
$$\left. - \frac{1}{\sqrt{6}}|1/2\ 1\ -1/2\rangle_P\right]e^{-i\omega_2 t} + 0\left[\frac{1}{\sqrt{2}}|-3/2\ 1\ -1/2\rangle_P - \frac{1}{2}|-3/2\ 0\ 1/2\rangle_P\right.$$
$$\left. - \frac{1}{2\sqrt{3}}|1/2\ 0\ 1/2\rangle_P + \frac{1}{\sqrt{6}}|-1/2\ -1\ 1/2\rangle_P\right]e^{-i\omega_2 t} + |S_R\rangle\,. \tag{4.4}$$

In the above equation, M' and $|S_R\rangle$ have the analogous meaning as M and $|S_L\rangle$ in Eq. (4.3).

The form of the superposition states $|\psi_L\rangle$ and $|\psi_R\rangle$ are very similar. Up to this point, however, the phase factors of the kets in the superposition states have not been specified. In general the coefficients a through c' are complex quantities. As will be seen shortly, the phase factors that are responsible for the appearance of oscillations in the polarization grating and absence in the population grating are the a–c phase relationship and the a'–c' phase relationship. In the population grating, the magnitude of the signal depends upon the global phase differences between rcp and lcp superposition states. The phase factors of the b and b' coefficients can be shown not to affect the time dependent observables. The terms in Eqs. (4.3) and (4.4) with coefficients b and b' will be labeled $|P_L\rangle$ and $|P_R\rangle$, respectively.

The phase factors can be explicitly incorporated into $|\psi_L\rangle$ by recasting a and c as $a\,e^{-i\phi_1}$ and $c\,e^{-i\phi_3}$. From Eq. (4.3), $|\psi_L\rangle$ can be rewritten in the following form:

$$|\psi_L\rangle = \sqrt{2}\,M\left[\cos\left(\frac{\Delta\omega t}{2}+\frac{\phi_L}{2}\right)|-1/2\ 0\ 1/2\rangle_S\right.$$
$$- i\sin\left(\frac{\Delta\omega t}{2}+\frac{\phi_L}{2}\right)$$
$$\left.\times|1/2\ 0\ -1/2\rangle_S\right]e^{-i(\Omega t+\Phi_L)} + |S_L\rangle + |P_L\rangle\,. \tag{4.5}$$

In Eq. (4.5), $\phi_L \equiv \phi_3 - \phi_1$, $\Phi_L \equiv (\phi_1+\phi_3)/2$, $\Omega = (\omega_1+\omega_3)/2$. [See Eq. (4.3).] A similar expression is obtained for $|\psi_R\rangle$:

$$|\psi_R\rangle = \sqrt{2}\,M\left[\cos\left(\frac{\Delta\omega t}{2}+\frac{\phi_R}{2}\right)\right.$$
$$\times|-1/2\ 0\ 1/2\rangle_S - i\sin\left(\frac{\Delta\omega t}{2}+\frac{\phi_R}{2}\right)$$
$$\left.\times|1/2\ 0\ -1/2\rangle_S\right]e^{-i(\Omega t+\Phi_R)} + |S_R\rangle + |P_R\rangle\,. \tag{4.6}$$

In obtaining Eq. (4.6), $a' \equiv a\,e^{-i\phi_1'}$ and $c' \equiv c\,e^{-i\phi_3'}$, and ϕ_R and Φ_R are analogous to ϕ_L and Φ_L. Since the strengths of the fields are identical in the lcp and rcp regions of the grating it is reasonable to take the magnitudes of the rcp and lcp coefficients to be the same. Consequently, the modulation depth factors in Eqs. (4.5) and (4.6) are equivalent. Also, the relative phases of the b and b' coefficients have not been specified since they are of no consequence.

At this point, one needs to consider the interaction of a linear probe with the rcp and lcp superposition states $|\psi_R\rangle$ and $|\psi_L\rangle$. The probe will be taken to be a delta function in time with $\sim 0°$ flip angle to avoid complications arising from the system evolution while the probe pulse is in the sample. The probe is now resolved into lcp and rcp components. First consider the interaction of the lcp component of the probe with $|\psi_L\rangle$. An lcp E field drives $|\psi_L\rangle$ through the coupling of the states $|-1/2\ 0\ 1/2\rangle_S$ and $|-1/2\ -1\ 1/2\rangle_P$. Note that the ΔM selection rule and orthogonality of the nuclear and electronic spin wave functions prevents any other couplings. The probability of absorption of lcp light by an atom in the state $|\psi_L\rangle$, P_{LL}, is proportional to the difference between the squares of the magnitudes of the coefficients for the states $|-1/2\ 0\ 1/2\rangle_S$ and $|-1/2\ -1\ 1/2\rangle_P$. The quantities are obtained by using the appropriate projection operators on $|\psi_L\rangle$ [Eqs. (4.3b) and (4.5)]. Thus,

$$P_{LL} = \langle\psi_L|-1/2\ 0\ 1/2\rangle_S\,{}_S\langle -1/2\ 0\ 1/2|\psi_L\rangle$$
$$- \langle\psi_L|-1/2\ -1\ 1/2\rangle_P\,{}_P\langle -1/2\ -1\ 1/2|\psi_L\rangle$$
$$= |\sqrt{2}\,M\cos\left(\frac{\Delta\omega t}{2}+\frac{\phi_L}{2}\right)e^{-(\Omega t+\phi_L)}$$
$$+ \langle S_L|-1/2\ 0\ 1/2\rangle_S|^2$$
$$- |\langle P_L|-1/2\ -1\ 1/2\rangle_P|^2\,. \tag{4.7}$$

The evaluation of Eq. (4.7) requires a specific form for $|S_L\rangle$. Although $|S_L\rangle$ depends on the relative magnitudes of a and c, the functional form of the diffraction efficiency is independent of whether $a \geqslant c$ or $a \leqslant c$. For the purposes of this discussion, the case in which $a \geqslant c$ will be evaluated. For this situation, $|S_L\rangle$ has the form

$$|S_L\rangle = \frac{|a-c|}{\sqrt{2}}[|-1/2\ 0\ 1/2\rangle$$
$$- |1/2\ 0\ -1/2\rangle]\,e^{-i(\omega_1 t+\phi_1)}\,. \tag{4.8}$$

Using the definitions given previously for Ω, $\Delta\omega$, Φ_L, and ϕ_L ($\Omega - \omega_1 = \Delta\omega$ and $\Phi_L - \phi_1 = \phi_L$), evaluation of Eq. (4.7) now leads to

$$P_{LL} = 2M\,[M + |a-c|]\cos^2\left(\frac{\Delta\omega t}{2}+\frac{\phi_L}{2}\right)$$
$$+ \frac{|a-c|^2}{2} - \frac{|b|^2}{6}\,. \tag{4.9}$$

Equation (4.9) illustrates that the absorption probability P_{LL} oscillates at the hyperfine frequency. This type of phenomenon has been seen by Ducas *et al.*[45] in a sodium absorption experiment in which a coherent superposition of $^2P_{1/2}$ levels was generated. The analysis presented here is partly based on their results.

Now consider the effect of the rcp component of the probe on the superposition $|\psi_R\rangle$ formed in the rcp grating region. The transition occurs because of the coupling of the states $|1/2\ 0\ -1/2\rangle_S$ and $|1/2\ 1\ -1/2\rangle_P$. The probability of absorption for this interaction is obtained in a manner analogous to P_{LL} using projection operators for the coupled states [see Eqs. (4.4) and (4.6) for $|\psi_R\rangle$]. $|S_R\rangle$ is defined for $a \gg c$ as follows:

$$|S_R\rangle = \frac{|a-c|}{\sqrt{2}}[\,|-1/2\ 0\ 1/2\rangle_S - |1/2\ 0\ -1/2\rangle_S\,]\, e^{-i(\omega_1 t+\phi_1')}. \tag{4.10}$$

By using the definitions of Ω, $\Delta\omega$, Φ_R, and ϕ_R, one can evaluate P_{RR}

$$P_{RR} = 2M\,[M+|a-c|]\sin^2\left(\frac{\Delta\omega t}{2}+\frac{\phi_R}{2}\right) + \frac{|a-c|^2}{2} - \frac{|b'|^2}{6}. \tag{4.11}$$

Two additional interactions still need to be accounted for. They are the absorption probability of the lcp probe component by the rcp grating region P_{LR} and the absorption probability of the rcp probe component by the lcp grating region P_{RL}.

$$\begin{aligned} P_{LR} &= \langle\psi_R|-1/2\ 0\ 1/2\rangle_S\,{}_S\langle-1/2\ 0\ 1/2|\psi_R\rangle \\ &\quad - \langle\psi_R|-1/2\ -1\ 1/2\rangle_P\,{}_P\langle-1/2\ -1\ 1/2|\psi_R\rangle \\ &= 2M\,[M+|a-c|]\cos^2\left(\frac{\Delta\omega t}{2}+\frac{\phi_R}{2}\right)+\frac{|a-c|^2}{2}, \end{aligned} \tag{4.12}$$

$$\begin{aligned} P_{RL} &= \langle\psi_L|1/2\ 0\ -1/2\rangle_S\,{}_S\langle1/2\ 0\ -1/2|\psi_L\rangle \\ &\quad - \langle\psi_L|1/2\ 1\ -1/2\rangle_P\,{}_P\langle1/2\ 1\ -1/2|\psi_L\rangle \\ &= 2M\,[M+|a-c|]\sin^2\left(\frac{\Delta\omega t}{2}+\frac{\phi_L}{2}\right)+\frac{|a-c|^2}{2}. \end{aligned} \tag{4.13}$$

The diffraction efficiency of an excited state grating results from the contributions of a phase and amplitude (absorption) component. Because the grating is being probed on resonance with the electronic transitions, a phase grating contribution to the diffraction efficiency will vanish.[8] The diffraction efficiency for an E field impinging on an amplitude (absorption) grating is determined by the peak-null difference in the optical density (OD).[8,25] (The diffracted intensity is proportional to the square of the peak-null difference in OD.) For the lcp probe component, the lcp grating regions serve as the peaks while the rcp grating regions serve as the nulls. The diffraction efficiency for the lcp probe component is proportional to the difference between the results of Eqs (4.9) and (4.12):

$$\eta_{\rm lcp} \propto P_{LL} - P_{LR}, \tag{4.14a}$$

$$\eta_{\rm lcp} \propto 2M\,[M+|a-c|]\sin\left[\Delta\omega t+\frac{\phi_L+\phi_R}{2}\right] \times\sin\left(\frac{\phi_R-\phi_L}{2}\right)-\frac{|b|^2}{6}. \tag{4.14b}$$

In a similar manner, the diffraction efficiency for the rcp probe component is obtained:

$$\eta_{\rm rcp} \propto P_{RR} - P_{RL}, \tag{4.15a}$$

$$\eta_{\rm rcp} \propto 2M\,[M+|a-c|]\sin\left[\Delta\omega t+\frac{\phi_L+\phi_R}{2}\right] \times\sin\left(\frac{\phi_R-\phi_L}{2}\right)-\frac{|b|^2}{6}. \tag{4.15b}$$

A comparison between Eqs. (4.14b) and (4.15b) shows that the diffraction efficiencies for the rcp and lcp E fields are the same. (Again, because of equal field strengths in the rcp and lcp regions of the grating, $|b|^2 = |b'|^2$.) Both fields are modulated at the hyperfine frequency $\Delta\omega$. The depth of modulation is dependent upon M and the difference between the phase angles ϕ_R and ϕ_L.

If an incident E field, $\mathbf{E}_i = \mathbf{E}_{\rm lcp} + \mathbf{E}_{\rm rcp}$ impinges on the grating, the E field that is diffracted is

$$\mathbf{E}_s = A\,[\,\eta_{\rm lcp}\mathbf{E}_{\rm lcp} + e^{i\theta}\eta_{\rm rcp}\mathbf{E}_{\rm rcp}\,]. \tag{4.16}$$

In Eq. (4.16), A is a constant that is dependent upon experimental parameters such as the beam geometries and sample OD, and θ is the spatial phase difference between the lcp and rcp grating. The phase angle $\theta = (2\pi/d)(x_{\rm rcp} - x_{\rm lcp})$, where $x_{\rm rcp}$ and $x_{\rm lcp}$ are the spatial positions of the rcp and lcp peaks and d is the fringe spacing. In the case considered here, $\theta = \pi$. Hence,

$$\mathbf{E}_s = A\eta_{\rm E}\,[\,\mathbf{E}_{\rm lcp} - \mathbf{E}_{\rm rcp}\,], \tag{4.17a}$$

$$\eta_{\rm E} = 2M^2\sin\left[\Delta\omega t+\frac{\phi_L+\phi_R}{2}\right]\sin\left(\frac{\phi_R-\phi_L}{2}\right)-\frac{|b|^2}{6}. \tag{4.17b}$$

Equation (4.17b) illustrates that the signal E field is linear, but rotated by 90° with respect to the incident field $\mathbf{E}_i$, and modulated at the hyperfine frequency. Also note that if the sample is completely in the ground state, i.e., $a = 1$ and $b = c = 0$, Eq. (4.17b) yields $\eta_{\rm E} = 0$.

To this point in the development, $\phi_R - \phi_L$ could take on any value, except for even multiples of π, and yield a modulated grating signal. However, a maximum modulation in the signal results when $\phi_R - \phi_L = \pm\pi$. Furthermore, since a maximum in the signal occurs at $t = 0$ (see Figs. 9–11), $\phi_L + \phi_R = \pm\pi$. (Note that the signal intensity is proportional to $\eta_{\rm E}^2$.) These conditions give solutions $\phi_R = 0$ and $\phi_L = \pm\pi$. Other solutions can be obtained by adding or subtracting 2π from ϕ_L and/or ϕ_R. The possible values of ϕ_L and ϕ_R range from -4π to $+4\pi$. In view of this discussion, the maximum modulation in the diffraction efficiency is observed when

$$\eta_{\rm E} = -2M^2\cos\Delta\omega t - \frac{|b|^2}{6}. \tag{4.17c}$$

A similar analysis of the population grating diffraction efficiency will result in the complete cancellation of the modulations for particular values of ϕ_L and ϕ_R. In a population grating, the peaks are excited by linearly polarized light, and the nulls are unexcited. In the peaks, the system is driven by both lcp and rcp light simultaneously ($\Delta M_F = \pm 1$). If the system starts in the same initial state as before, $|10\rangle_S$, the resulting superposition state has a form which is a linear combination of $|\psi_L\rangle$ and $|\psi_R\rangle$. However, the values of the phase angles ϕ_1, ϕ_1', ϕ_3, and ϕ_3' are not necessarily the same as in the polarization grating:

$$|\psi_0\rangle = \frac{1}{\sqrt{2}}(|\psi_L\rangle + |\psi_R\rangle)$$
$$= \frac{1}{\sqrt{2}}\left[(a+a')|10\rangle_S\, e^{-i\omega_1 t} + b\,|11\rangle_P\, e^{-i\omega_2 t} + b'|1\ -1\rangle_P\, e^{-i\omega_2 t} + (c+c')|20\rangle_S\, e^{-i\omega_3 t}\right]. \tag{4.18}$$

Note that $|\psi_0\rangle$ is a superposition of four states, while $|\psi_R\rangle$ and $|\psi_L\rangle$ are superpositions of only three states.

Rewriting Eq. (4.18) in the uncoupled representation leads to a form which is a composite of Eqs. (4.5) and (4.6):

$$|\psi_0\rangle = M\left[\left(\cos\left(\frac{\Delta\omega t}{2}+\frac{\phi_L}{2}\right)e^{i\phi_0} + \cos\left(\frac{\Delta\omega t}{2}+\frac{\phi_R}{2}\right)e^{-i\phi_0}\right)|-1/2\ 0\ 1/2\rangle_S - i\left(\sin\left(\frac{\Delta\omega t}{2}+\frac{\phi_L}{2}\right)e^{i\phi_0} + \sin\left(\frac{\Delta\omega t}{2}+\frac{\phi_R}{2}\right)e^{-i\phi_0}\right)|1/2\ 0\ -1/2\rangle_S\right] e^{-i(\Omega t+\Phi_0)} + \frac{1}{\sqrt{2}}\left[|S_L\rangle + |S_R\rangle + |P_L\rangle + |P_R\rangle\right]. \tag{4.19}$$

In Eq. (4.19), $\Phi_0 \equiv (\Phi_L + \Phi_R)/2$ and $\phi_0 \equiv (\Phi_R - \Phi_L)/2$. The sodium atoms in the nulls of the grating are taken to be in the ground eigenstate $|10\rangle_S$:

$$|\psi_N\rangle = |10\rangle_S\, e^{-i\omega_1 t}$$
$$= \frac{1}{\sqrt{2}}\left[|-1/2\ 0\ 1/2\rangle_S - |1/2\ 0\ -1/2\rangle_S\right] e^{-i\omega_1 t}. \tag{4.20}$$

The grating diffraction efficiency will be analyzed in the same manner as before. The probe will be decomposed into a right and left component and the peak-null difference in the absorption probability will be evaluated for each component. The absorption probabilities for the lcp and rcp probe components in the peaks are

$$P_{L,0} = |\langle\psi_0|-1/2\ 0\ 1/2\rangle_S|^2 - |\langle\psi_0|-1/2\ -1\ 1/2\rangle_P|^2, \tag{4.21}$$

$$P_{R,0} = |\langle\psi_0|1/2\ 0\ -1/2\rangle_S|^2 - |\langle\psi_0|1/2\ 1\ -1/2\rangle_P|^2. \tag{4.22}$$

The corresponding terms for the null regions are

$$P_{L,N} = |\langle\psi_N|-1/2\ 0\ 1/2\rangle_S|^2 - |\langle\psi_N|-1/2\ -1\ 1/2\rangle_P|^2, \tag{4.23}$$

$$P_{R,N} = |\langle\psi_N|1/2\ 0\ -1/2\rangle_S|^2 - |\langle\psi_N|1/2\ 1\ -1/2\rangle_P|^2. \tag{4.24}$$

The diffraction efficiencies for the two probe components are calculated from Eqs. (4.19)–(4.24). Again, to define $|S_L\rangle$ and $|S_R\rangle$, the condition that $a \geqslant c$ is adopted [see Eqs. (4.8) and (4.10)]:

$$\eta_{\rm lcp} \propto P_{L,0} - P_{L,N}, \tag{4.25a}$$

$$\eta_{\rm lcp} \propto M^2\left[\cos^2\left(\frac{\Delta\omega t}{2}+\frac{\phi_L}{2}\right) + \cos^2\left(\frac{\Delta\omega t}{2}+\frac{\phi_R}{2}\right) + 2\cos\left(\frac{\Delta\omega t}{2}+\frac{\phi_L}{2}\right)\cos\left(\frac{\Delta\omega t}{2}+\frac{\phi_R}{2}\right)\cos 2\phi_0\right] + 2M|a-c|\cos\bar{\phi}\left[\cos\left(\frac{\Delta\omega t}{2}+\frac{\phi_L}{2}\right)\cos\left(\frac{\Delta\omega t}{2}+\Phi_L-\bar{\Phi}\right) + \cos\left(\frac{\Delta\omega t}{2}+\frac{\phi_R}{2}\right)\cos\left(\frac{\Delta\omega t}{2}+\Phi_R-\bar{\Phi}\right)\right] + |a-c|^2\cos^2\bar{\phi} - \frac{|b|^2}{12} - 1/2. \tag{4.25b}$$

In the above expression, $\bar{\phi}$ is one-half the global phase difference between $|\psi_R\rangle$ and $|\psi_L\rangle$; $\bar{\phi} \equiv (\phi_1' - \phi_1)/2$, where ϕ_1' and ϕ_1 are phase angle of the coefficients a' and a [see Eqs. (4.1) and (4.2)]. The angle $\bar{\Phi}$ is the average global phase factor given by $(\phi_1' + \phi_1)/2$:

$$\eta_{\rm rcp} \propto P_{R,0} - P_{R,N}, \tag{4.26a}$$

$$\eta_{\rm rcp} \propto M^2\left[\sin^2\left(\frac{\Delta\omega t}{2}+\frac{\phi_L}{2}\right) + \sin^2\left(\frac{\Delta\omega t}{2}+\frac{\phi_R}{2}\right) + 2\sin\left(\frac{\Delta\omega t}{2}+\frac{\phi_L}{2}\right)\sin\left(\frac{\Delta\omega t}{2}+\frac{\phi_R}{2}\right)\cos 2\phi_0\right] + 2M|a-c|\cos\bar{\phi}\left[\sin\left(\frac{\Delta\omega t}{2}+\frac{\phi_L}{2}\right)\sin\left(\frac{\Delta\omega t}{2}+\Phi_L-\bar{\Phi}\right) + \sin\left(\frac{\Delta\omega t}{2}+\frac{\phi_R}{2}\right)\sin\left(\frac{\Delta\omega t}{2}+\Phi_R-\bar{\Phi}\right)\right] + |a-c|^2\cos^2\bar{\phi} - \frac{|b|^2}{12} - 1/2. \tag{4.26b}$$

In deriving Eqs. (4.25b) and (4.26b), it is again reasonable to take $|b|^2 = |b'|^2$.

In the experiment, the observed diffracted signal from the population grating does not possess any modulations and is linearly polarized parallel to the probe at all times. Hence, $\eta_{\rm lcp}$ must equal $\eta_{\rm rcp}$ and both must be independent of time. This condition restricts the values of the phase angles ϕ_L and ϕ_R (the phase angles between a–c and a'–c') and ϕ_0 [the average phase difference given by $(\Phi_L - \Phi_R)/2$]. A consistent solution for $\eta_{\rm lcp}$ and $\eta_{\rm rcp}$ can be obtained by setting ϕ_0 equal to 0 ($\Phi_L = \Phi_R$) and $\phi_L/2 = \phi_R/2 \pm \pi$ ($\phi_L - \phi_R = \pm 2\pi$):

$$\eta_{\rm lcp} = \eta_{\rm rcp} = |a-c|^2 \cos^2 \bar{\phi} - \frac{|b|^2}{12} - 1/2 . \quad (4.27)$$

The diffracted E field for the population grating is [see also Eq. (4.16)]

$$\mathbf{E}_s = A\,[\eta_{\rm lcp}\mathbf{E}_{\rm lcp} + e^{i\theta}\eta_{\rm rcp}\mathbf{E}_{\rm rcp}] . \quad (4.28)$$

For $\theta = 0$ (there is no spatial phase shift) Eq. (4.28) becomes

$$\mathbf{E}_s = A\eta_{\mathbf{E}}\,[\mathbf{E}_{\rm lcp} + \mathbf{E}_{\rm rcp}] , \quad (4.29a)$$

where $\eta_{\mathbf{E}}$ is given by Eq. (4.27). Thus, the diffracted signal has no modulations and is linearly polarized with the same polarization as the incident probe. As an additional consideration, the diffraction efficiency must go to zero when the system is in the ground state ($a = 1, b = c = 0$). Hence, the global phase difference $\bar{\phi}$ must equal an odd multiple of $\pi/4$. Consequently,

$$\eta_{\mathbf{E}} = \frac{|a-c|^2}{2} - \frac{|b|^2}{12} - 1/2 . \quad (4.29b)$$

It is worthwhile to summarize the polarization and population grating results. The analysis of the polarization grating indicated that in order for modulations to occur, $\phi_R - \phi_L$ could not equal an even multiple of π. A maximum in the signal modulation depth would be observed if $\phi_R - \phi_L = \pm\pi$. (Since the modulations in the grating decays were rather large, it was not unreasonable to propose that $\phi_R - \phi_L = \pm\pi$.) The condition for maximum modulation, coupled with the fact that the diffracted signal intensity is a maximum at $t = 0$, led to the solutions $\phi_R = 0$ and $\phi_L = \pm\pi$. For the population grating, the absence of oscillations in the diffracted signal and the fact that the signal is linearly polarized at all times yielded the relations $\Phi_R = \Phi_L$ and $\phi_R - \phi_L = \pm 2\pi$.

An additional phase angle condition that was obtained in the population grating analysis stemmed from the fact the grating diffraction efficiency must be identically zero if the system is in the ground state. This requirement gave a limited set of values for the global phase difference between the right and left component wave functions. The phase difference was found to be $\phi_0 = \pm\pi/4, \pm 3\pi/4$. ($\phi_0$ was not a factor in the polarization grating analysis.) From the possible values of ϕ_R, ϕ_L, Φ_R, Φ_L, ϕ_0, and $\bar{\phi}$, one can obtain a particular solution for the phase angles of the right (ϕ_1', ϕ_3') and left (ϕ_1, ϕ_3) components of ψ_0. If ϕ_1' is set equal to zero then $\phi_1' \equiv 0$, $\phi_3' \equiv \pi/2$, $\phi_1 = 3\pi/2$, and $\phi_3 = -\pi$. By comparison, the phase angle requirement in the polarization grating does not yield a single set of angles if $\phi_1' \equiv 0$. This is because the global phase difference between $|\psi_R\rangle$ and $|\psi_L\rangle$ is unimportant in this case. If ϕ_1' and ϕ_1 are both arbitrarily set equal to zero, then the polarization grating solution is $\phi_1' \equiv 0$, $\phi_3' = 0$, $\phi_1 \equiv 0$, and $\phi_3 = -\pi$.

A simple interpretation of the above results is as follows. In the polarization grating, the excitations produce rcp and lcp grating regions, characterized by right and left wave functions, that are spatially separated. Because of this spatial separation the rcp and lcp grating regions contribute independently to the grating signal in the sense that there is no need to specify a particular global phase relationship. However, the internal phase factors between the ground state kets for $|\psi_R\rangle$ and $|\psi_L\rangle$ differ by a factor of $\pm\pi$ (for the condition of maximum modulation.) This shows that rcp and lcp light from the grating excitations drive the sodium atom transitions 180° out of phase with each other. This phase shift manifests itself in the time dependent absorption probabilities of the two grating regions which oscillate out of phase by π. Since the out-of-phase components are spatially separated by half a grating fringe and the lcp and rcp probe components sample the peak-null (half-fringe spacing) *difference* in absorption probability, the diffracted signal exhibits oscillations.

On the other hand, the interpretation of the population grating is different. It might at first seem plausible to simply add the contributions of the out-of-phase components from the polarization grating since there is no spatial separation between the rcp and lcp grating regions. This simple addition would appear to cause a cancellation in the oscillations. However, the results showed that this is not the case since $\phi_R - \phi_L = \pm 2\pi$ and not $\pm\pi$. Unlike the three state superpositions of the polarization grating, the wave functions generated in the population grating contain four states. This puts different constraints on the population grating solution which give rise to a different relationship between ϕ_L and ϕ_R. Consequently, the experimental results demonstrate that the interaction of a sodium atom with linearly polarized light is not equivalent to the sum of separate interactions of the atom with rcp and lcp light.

It should be emphasized that the particular solutions obtained for the phase angles were derived from the consideration of a limited number of states and from the coherence generated between the $|10\rangle_S$ and $|20\rangle_S$ states. Somewhat different results would be obtained from coherence between the $|11\rangle_S$, $|21\rangle_S$ and the $|1-1\rangle_S$, $|2-1\rangle_S$ pairs. Although the phase differences ϕ_R and ϕ_L should be the same, the global factors and the absolute values of $\phi_1 - \phi_3'$ would be different. This results from the fact that the magnitudes of the Clebsch–Gordan are different from kets other than $|10\rangle_S$ and $|20\rangle_S$.

In addition to the ground state hyperfine interaction, the excited state hyperfine interaction also affects the signal. The influence of the upper state splitting is evident in Fig. 10 where the probe and excitation are tuned into the $^2P_{1/2}$ manifold. The excitation pulses generate coherences between both the ground and excited state hyperfine states. In the analysis given above a minimum set of states was used in order to illustrate the principal effects. If a sodium atom

starts in the $|10\rangle_S$ state, a lcp excitation field will actually generate the following superposition:

$$|\psi_L\rangle = a|10\rangle_S\, e^{-i\omega_1 t} + b_1|1-1\rangle_P\, e^{-i\omega_2 t} + b_2|2-1\rangle_P\, e^{-i\omega_4 t} + c|20\rangle_S\, e^{-i\omega_3 t} + 0|11\rangle_P\, e^{-i\omega_2 t} + 0|21\rangle_P\, e^{-i\omega_4 t}. \quad (4.30)$$

The superposition states discussed earlier, such as Eq. (4.1), omitted the additional excited states.

The excited state splitting is only observed when the probe pulse encounters a time dependent optical density variation resulting from the time evolution of the coherently prepared excited $|m_I m_l m_s\rangle$ states. If the excitation pulses excite the $^2P_{1/2}$ states, a probe which is tuned into the $^2P_{3/2}$ manifold will not be sensitive to the $^2P_{1/2}$ coherence. Consequently, no modulation corresponding to the excited hyperfine splitting is observed. This is why the nondegenerate (two color) polarization grating experiment has the same envelope as the population grating (Fig. 9), while the degenerate (one color) polarization grating experiment has the additional low frequency oscillation (Fig. 10).

So far this discussion has explained why there are oscillations in the polarization grating data and not in the population grating data, and why the degenerate polarization grating experiment displays the excited state hyperfine frequency while the nondegenerate experiment does not. The final point that needs to be addressed concerns the fact that the modulations are less pronounced in the $^2P_{3/2}$ polarization grating than in the $^2P_{1/2}$ case. As was shown earlier, the modulations stem from the oscillation of the $|m_I m_l m_s\rangle$ character of the ground state superpositions. This oscillation led to a time dependent absorption probability for lcp and rcp light. However, the $^2P_{3/2}$ manifold contains more $|m_I m_l m_s\rangle$ states in the expansion than does the $^2P_{1/2}$ manifold. This leads to additional transition pathways from the ground state kets which wash out the oscillations. An analysis similar to that given above for the $^2P_{1/2}$ state was performed for the $^2P_{3/2}$ state. Oscillations in probability between ground state hyperfine kets, $|m_I m_l m_s\rangle$ occur [analogous to Eqs. (4.5) and (4.6)]. However, both of the kets involved are coupled to $^2P_{3/2}$ states by the probe. Consequently, there is no oscillation in transition probability and no contribution from these kets to a modulated grating signal. This cancellation of the modulation in transition probability can be shown to occur for all the $^2S_{1/2} \rightarrow {}^2P_{3/2}$ transitions except for those involving the $|2-1\rangle_{P'}$ and $|21\rangle_{P'}$ states. Another factor which reduces the observed modulation depth for the $^2P_{3/2}$ data from that of the $^2P_{1/2}$ data, is that the $^2SP_{1/2} \rightarrow {}^2P_{3/2}$ transition contains two additional pathways which do not involve coherences between ground state hyperfine levels. These pathways, which originate from $|2-2\rangle_S$ and $|2\,2\rangle_S$, contribute to the grating signal but not to the modulation.

The factors which reduce the modulation depth of the ground state hyperfine oscillations in the $^2P_{3/2}$ experiment do not apply to the excited state hyperfine oscillations. Consequently, the effect of the lower frequency modulation in the $^2P_{3/2}$ and $^2P_{1/2}$ grating signal decays are comparable. A comparison of Figs. 10 and 11 shows that the envelopes for the decays at the two different wavelengths are similar although the complex hyperfine structure of the $^2P_{3/2}$ manifold is not resolved.

The analysis of the sodium grating experiments has explained the origin and nature of the oscillations observed in the polarization grating signal. A small subset of all the possible states was considered in order to demonstrate the importance of the phase factors in generating the oscillations in the polarization grating and cancelling the oscillations in the population grating. The theory predicts that one should see a power dependence in the modulation depth. This was not observed experimentally since the Rabi angles of the excitation pulses even at the lowest powers (100 nJ) were still on the order of 7π. A more detailed analysis of the sodium grating experiments would include the interaction between all possible states connected by the excitation fields. For most purposes the results obtained by considering the system to start in different eigenstates can simply be added.

Finally, in these calculations the probe pulse is taken to be very weak. Because of the large Na transition moments, an atom can undergo several optical nutations during the time the probe is in the sample. This would cause the signal pulse envelope to be modulated at the Rabi frequency. The linear probe would also tend to mix the initial superposition states. However, the overall integrated intensity of the diffracted signal as a function of probe delay should only be dependent upon the time evolution of the states prepared by the excitation pulses before the probe pulse arrives. To study the time resolved signal pulse envelope or the absolute diffraction efficiency, it is necessary to perform a more detailed analysis than presented here.

V. CONCLUDING REMARKS

This paper has described the application of picosecond transient grating experiments to the investigation of gas phase dynamics and spectroscopy. First, in the Na experiments, it was demonstrated that in the absence of collisions on the experimental time scale (a few nanoseconds), the grating signal is related to the Fourier transform of the velocity distribution. The experiment does not require the observation of resolvable spectral lines and therefore can be applied in situations where Doppler linewidth spectroscopy is not possible. While a thermal equilibrium sample was investigated, the method is not limited to equilibrium systems. For example, if molecule AB is photodissociated to A + B with grating excitation conditions, a probe tuned to an A fragment absorption will yield the A velocity distribution. The probe can be tuned into a B absorption, and the B velocity distribution measured. Another application is the study of the evolution of velocity distributions when a system is perturbed from equilibrium. If a perturbation occurs at $t = 0$ in a low pressure system, collisions will return the system to equilibrium. Transient grating decays mesured at various times after $t = 0$ can monitor the evolution of the velocity distribution.

In addition to the collision free Na experiments, the I_2 studies demonstrated the ability of the grating experiment to examine the effects of collisions on excited molecules. The signal contains information concerning the initial velocity

distribution, the effect of the collisions, and the velocity distribution following a state changing collision. The experiments on I_2 showed that a collision of an exited I_2 molecule with ground state I_2 molecule can result in a change of state of the excited collision partner. The new state absorbs strongly at 532 nm. The cross section for this process is somewhat smaller than hard sphere, and the initial velocity is randomized by the collision. In terms of studying collisional kinetics, the grating method inherently establishes a well-defined distance scale (determined by the fringe spacing) which provides an extra dimension in the measurement. State populations and spatial distribution functions are probed simultaneously.

The application of the polarization grating method to Na vapor demonstrates the possibility of obtaining Doppler free, high resolution spectroscopic information from a time domain technique. In Na, atomic hyperfine splittings were observed. However, the same approach should be useful whenever $\Delta M = \pm 1$ angular momentum selection rules are obeyed. Thus, the polarization grating could prove useful in the investigation of vibronic rotational state dynamics and dephasing.

Finally, the transient grating method has other attributes which could prove useful in a number of situations. Since the grating measurement is performed on a small volume, the technique could be employed to investigate the macroscopic anisotropy of large systems. Furthermore, the grating signal is a coherent beam, which is generally more readily detectable in an adverse environment than a signal generated by conventional spectroscopic methods. The combination of these features should make gas phase picosecond transient grating experiments useful in the examination of combustion, flames, and plasmas, and in a wide variety of gas phase problems.

ACKNOWLEDGMENTS

This work was supported by the National Science Foundation, Division of Materials Research No. DMR 84-16343 and additional support was provided by the Office of Naval Research No. N00014-85-K-0409. Todd S. Rose would like to thank IBM for a one year graduate fellowship; William L. Wilson would like to thank AT&T Bell Laboratories for a full graduate fellowship; and Gerhard Wäckerle would like to thank the Deutsche Forschungsgemeinschaft for partial support.

APPENDIX

The expansion of the coupled sodium $|FM_F\rangle$ states ($3S$ and $3P$) in terms of the $|m_I m_l m_s\rangle$ states is listed below. The Clebsch–Gordan coefficients were derived by raising and lowering operator techniques:

$^2S_{1/2}$:

$$|2\ 2\rangle = |3/2\ 0\ 1/2\rangle,$$
$$|2\ 1\rangle = \sqrt{3/4}\,|1/2\ 0\ 1/2\rangle + 1/2|3/2\ 0\ -1/2\rangle,$$
$$|2\ 0\rangle = 1/\sqrt{2}\,|-1/2\ 0\ 1/2\rangle + 1/\sqrt{2}\,|1/2\ 0\ -1/2\rangle,$$
$$|2\ -1\rangle = 1/2|-3/2\ 0\ 1/2\rangle + \sqrt{3/4}\,|-1/2\ 0\ -1/2\rangle,$$
$$|2\ -2\rangle = |-3/2\ 0\ -1/2\rangle,$$
$$|1\ 1\rangle = 1/2|1/2\ 0\ 1/2\rangle - \sqrt{3/4}\,|3/2\ 0\ -1/2\rangle,$$
$$|1\ 0\rangle = 1/\sqrt{2}\,|-1/2\ 0\ 1/2\rangle - 1/\sqrt{2}\,|1/2\ 0\ -1/2\rangle,$$
$$|1\ -1\rangle = \sqrt{3/4}\,|-3/2\ 0\ 1/2\rangle - 1/2|-1/2\ 0\ -1/2\rangle.$$

$^2P_{1/2}$:

$$|2\ 2\rangle = \sqrt{2/3}\,|3/2\ 1\ -1/2\rangle - 1/\sqrt{3}\,|3/2\ 0\ 1/2\rangle,$$
$$|2\ 1\rangle = 1/\sqrt{2}\,|1/2\ 1\ -1/2\rangle - 1/2|1/2\ 0\ 1/2\rangle + 1/\sqrt{12}\,|3/2\ 0\ -1/2\rangle + 1/\sqrt{6}\,|3/2\ -1\ 1/2\rangle,$$
$$|2\ 0\rangle = 1/\sqrt{3}\,|-1/2\ 1\ -1/2\rangle - 1/\sqrt{6}\,|-1/2\ 0\ 1/2\rangle + 1/\sqrt{6}\,|1/2\ 0\ -1/2\rangle - 1/\sqrt{3}\,|1/2\ -1\ 1/2\rangle,$$
$$|2\ -1\rangle = 1/\sqrt{6}\,|-3/2\ 1\ -1/2\rangle - 1/\sqrt{12}\,|-3/2\ 0\ 1/2\rangle + 1/2|-1/2\ 0\ -1/2\rangle - 1/\sqrt{2}\,|-1/2\ -1\ 1/2\rangle,$$
$$|2\ -2\rangle = 1/\sqrt{3}\,|-3/2\ 0\ -1/2\rangle - \sqrt{2/3}\,|-3/2\ -1\ 1/2\rangle,$$
$$|1\ 1\rangle = 1/\sqrt{6}\,|1/2\ 1\ -1/2\rangle - 1/\sqrt{12}\,|1/2\ 0\ 1/2\rangle - 1/2|3/2\ 0\ -1/2\rangle + 1/\sqrt{2}\,|3/2\ -1\ 1/2\rangle,$$
$$|1\ 0\rangle = 1/\sqrt{3}\,|-1/2\ 1\ -1/2\rangle - 1/\sqrt{6}\,|-1/2\ 0\ 1/2\rangle - 1/\sqrt{6}\,|1/2\ 0\ -1/2\rangle + 1/\sqrt{3}\,|1/2\ -1\ 1/2\rangle,$$

$$|1\ -1\rangle = 1/\sqrt{2}\,|-3/2\ 1\ -1/2\rangle - 1/2|-3/2\ 0\ 1/2\rangle$$
$$- 1/\sqrt{12}\,|-1/2\ 0\ -1/2\rangle + 1/\sqrt{6}\,|-1/2\ -1\ 1/2\rangle\,.$$

$^2P_{3/2}$:

$$|3\ 3\rangle = |3/2\ 1\ 1/2\rangle\,,$$
$$|3\ 2\rangle = 1/\sqrt{6}\,|3/2\ 1\ -1/2\rangle + 1/\sqrt{3}\,|3/2\ 0\ 1/2\rangle + 1/\sqrt{2}\,|1/2\ 1\ 1/2\rangle\,,$$
$$|3\ 1\rangle = \sqrt{2/15}\,|3/2\ 0\ -1/2\rangle + 1/\sqrt{15}\,|3/2\ -1\ 1/2\rangle$$
$$+ 1/\sqrt{5}\,|1/2\ 1\ -1/2\rangle + \sqrt{2/5}\,|1/2\ 0\ 1/2\rangle$$
$$+ 1/\sqrt{5}\,|-1/2\ 1\ 1/2\rangle\,,$$
$$|3\ 0\rangle = 1/\sqrt{20}\,|3/2\ -1\ -1/2\rangle + \sqrt{3/10}\,|1/2\ 0\ -1/2\rangle$$
$$+ \sqrt{3/20}\,|1/2\ -1\ 1/2\rangle + \sqrt{3/20}\,|-1/2\ 1\ -1/2\rangle$$
$$+ \sqrt{3/10}\,|-1/2\ 0\ 1/2\rangle + 1/\sqrt{20}\,|-3/2\ 1\ 1/2\rangle\,,$$
$$|3\ -1\rangle = 1/\sqrt{5}\,|1/2\ -1\ -3/2\rangle + \sqrt{2/5}\,|-1/2\ 0\ -1/2\rangle$$
$$+ 1/\sqrt{5}\,|-1/2\ -1\ 1/2\rangle + 1/\sqrt{15}\,|-3/2\ 1\ -1/2\rangle$$
$$+ \sqrt{2/15}\,|-3/2\ 0\ 1/2\rangle\,,$$
$$|3\ -2\rangle = 1/\sqrt{2}\,|-1/2\ -1\ -1/2\rangle + 1/\sqrt{3}\,|-3/2\ 0\ -1/2\rangle$$
$$+ 1/\sqrt{6}\,|-3/2\ -1\ 1/2\rangle\,,$$
$$|3\ -3\rangle = |-3/2\ -1\ -1/2\rangle\,,$$
$$|2\ 2\rangle = -1/\sqrt{6}\,|3/2\ 1\ -1/2\rangle - 1/\sqrt{3}\,|3/2\ 0\ 1/2\rangle + 1/\sqrt{2}\,|1/2\ 1\ 1/2\rangle\,,$$
$$|2\ 1\rangle = -1/\sqrt{3}\,|3/2\ 0\ -1/2\rangle - 1/\sqrt{6}\,|3/2\ -1\ 1/2\rangle + 1/\sqrt{2}\,|-1/2\ 1\ 1/2\rangle\,,$$
$$|2\ 0\rangle = -1/2|3/2\ -1\ -1/2\rangle - 1/\sqrt{6}\,|1/2\ 0\ -1/2\rangle - 1/\sqrt{12}\,|1/2\ -1\ 1/2\rangle$$
$$+ 1/\sqrt{12}\,|-1/2\ 1\ -1/2\rangle + 1/\sqrt{6}\,|-1/2\ 0\ 1/2\rangle$$
$$+ 1/2\,|-3/2\ 1\ 1/2\rangle\,,$$
$$|2\ -1\rangle = -1/\sqrt{2}\,|1/2\ -1\ -1/2\rangle + 1/\sqrt{6}\,|-3/2\ 1\ -1/2\rangle$$
$$+ 1/\sqrt{3}\,|-3/2\ 0\ 1/2\rangle\,,$$
$$|2\ -2\rangle = -1/\sqrt{2}\,|-1/2\ -1\ -1/2\rangle + 1/\sqrt{3}\,|-3/2\ 0\ -1/2\rangle$$
$$+ 1/\sqrt{6}\,|-3/2\ -1\ 1/2\rangle\,,$$
$$|1\ 1\rangle = \sqrt{1/5}\,|3/2\ 0\ -1/2\rangle + 1/\sqrt{10}\,|3/2\ -1\ 1/2\rangle$$
$$- \sqrt{2/15}\,|1/2\ 1\ -1/2\rangle - \sqrt{4/15}\,|1/2\ 0\ 1/2\rangle$$
$$+ \sqrt{3/10}\,|-1/2\ 1\ 1/2\rangle\,,$$
$$|1\ 0\rangle = \sqrt{9/20}\,|3/2\ -1\ -1/2\rangle - 1/\sqrt{30}\,|1/2\ 0\ -1/2\rangle$$
$$- 1/\sqrt{60}\,|1/2\ -1\ 1/2\rangle - 1/\sqrt{60}\,|-1/2\ 1\ -1/2\rangle$$
$$- 1/\sqrt{30}\,|-1/2\ 0\ 1/2\rangle + \sqrt{9/20}\,|-3/2\ 1\ 1/2\rangle\,,$$
$$|1\ -1\rangle = \sqrt{3/10}\,|1/2\ -1\ -1/2\rangle - \sqrt{4/15}\,|-1/2\ 0\ -1/2\rangle$$
$$- \sqrt{2/15}\,|-1/2\ -1\ 1/2\rangle$$
$$+ 1/\sqrt{10}\,|-3/2\ 1\ -1/2\rangle + 1/\sqrt{5}\,|-3/2\ 0\ 1/2\rangle\,,$$
$$|0\ 0\rangle = 1/2|3/2\ -1\ -1/2\rangle + 1/\sqrt{6}\,|1/2\ 0\ -1/2\rangle$$
$$+ 1/\sqrt{12}\,|1/2\ -1\ 1/2\rangle - 1/\sqrt{12}\,|-1/2\ 1\ -1/2\rangle$$
$$- 1/\sqrt{6}\,|-1/2\ 0\ 1/2\rangle + 1/2|-3/2\ 1\ 1/2\rangle\,.$$

[1](a) R. G. Brewer and R. L. Shoemaker, Phys. Rev. Lett. **27**, 631 (1971); R. G. Brewer and A. Z. Genack, *ibid.* **36**, 959 (1976); (b) P. R. Berman, T. W. Mossberg, and S. R. Hartmann, Phys. Rev. A **25**, 2550 (1982); R. Kachru, T. J. Chen, T. W. Mossberg, and S. R. Hartman, *ibid.* **25**, 1546 (1982); (c) A. H. Zewail, Acc. Chem. Res. **13**, 360 (1980), and references therein.

[2]W. Warren and M. A. Banash, *Coherence and Quantum Optics V* (Plenum, New York, 1984), p. 959; M. A. Banash and W. S. Warren, Laser Chem. **6**, 47 (1986).

[3]L. A. Ornstein and W. R. van Wijk, Z. Phys. **78**, 734 (1972).

[4]R. Vasudev, R. N. Zare, and R. N. Dixon, J. Chem. Phys. **80**, 4863 (1984).

[5]T. S. Rose, R. Righini, and M. D. Fayer, Chem. Phys. Lett. **106**, 13 (1984).

[6]J. K. Tyminski, R. C. Powell, and W. K. Zwicker, Phys. Rev. B **29**, 6074 (1984).

[7]V. J. Newell, T. S. Rose, and M. D. Fayer, Phys. Rev. B **32**, 8035 (1985).

[8]K. A. Nelson, R. Casalegno, R. J. D. Miller, and M. D. Fayer, J. Chem. Phys. **77**, 1144 (1982).

[9]A. B. Myers and R. M. Hochstrasser, J. Chem. Phys. **85**, 630 (1986).

[10]T. S. Rose and M. D. Fayer, Chem. Phys. Lett. **117**, 12 (1985).

[11]T. S. Rose, W. L. Wilson, G. Wäckerle, and M. D. Fayer (to be published).

[12]A. N. Nesmeyanov, *Vapor Pressure of the Elements* (Academic, New York, 1963).

[13]B. P. Kibble, G. Kopley, and L. Krause, Phys. Rev. **153**, 9 (1967).

[14]P. W. Atkins, *Physical Chemistry*, 2nd ed. (Oxford University, Oxford, 1982), p. 879.

[15]D. P. Shoemaker, C. W. Garland, and J. I. Steinfeld, *Exp. in Physical Chemistry*, 3rd ed. (McGraw–Hill, New York, 1974), p. 345.

[16]F. E. Stafford, J. Chem. Ed. **39**, 627 (1962).

[17]P. Luc, J. Mol. Spectrosc. **80**, 41 (1980).

[18]J. Tellinghuisen, J. Chem. Phys. **76**, 4736 (1982).

[19]I. A. Levine, *Physical Chemistry* (McGraw–Hill, New York, 1978), pp. 421, 597–8.

[20]A. H. Zewail, Acc. Chem. Res. **13**, 360 (1980).

[21]J. I. Steinfeld, J. Phys. Chem. **13**, 445 (1984).

[22]R. S. Mulliken, J. Chem. Phys. **55**, 228 (1971).

[23]L. J. Rothberg and N. Bloembergen, Phys. Rev. A **30**, 820 (1984).

[24]C. N. Cohen-Tannoudji, B. Diu, and F. Laloë, *Quantum Mechanics* (Wiley–Interscience, New York, 1977), p. 1254.

[25]A. Von Jena and H. E. Lessing, Opt. Quantum Elec. **11**, 419 (1979).

[26]G. Eyring and M. D. Fayer, J. Chem. Phys. **81**, 4314 (1984).

[27]W. L. Wiese, M. W. Smith, and B. M. Miles, *Atomic Transition Probabilities*, Natl. Bur. Stand. (U.S.) Circ. No. 2 (U.S. GPO, Washington, D.C., 1969).

[28]D. M. Bloom, P. F. Liao, and N. P. Economon, Opt. Lett. **3**, 58 (1978).

[29]L. M. Humphrey, J. P. Gordon, and P. F. Liao, Opt. Lett. **5**, 56 (1980).

[30]J. P. Woerdman and M. F. H. Schuurmans, Opt. Lett. **6**, 239 (1981).

[31]S. N. Jabr, L. K. Lam, and R. W. Hellwarth, Phys. Rev. A **24**, 3264 (1981).

[32]P. Kumar, Opt. Lett. **10**, 74 (1985).

[33]T. Mossberg, A. Flusberg, R. Kachru, and S. R. Hartmann, Phys. Rev. Lett. **39**, 1523 (1977).

[34]A. Flusberg, T. Mossberg, R. Kachru, and S. R. Hartmann, Phys. Rev. Lett. **41**, 305 (1978).

[35]T. Mossberg, A. Flusberg, R. Kachru, and S. R. Hartman, Phys. Rev. Lett. **42**, 1665 (1979).

[36]T. W. Mossberg, R. Kachru, E. Whittaker, and S. R. Hartmann, Phys. Rev. Lett. **43**, 851 (1979).

[37](a) M. Fujita, H. Nakatsuka, H. Nakanishi, and M. Matsuoka, Phys. Rev. Lett. **42**, 974 (1979); (b) R. K. Jain, H. W. K. Tom, and J. C. Diels, *Picosecond Phenomena III*, edited by K. B. Eisenthal, *et al.* (Springer, Berlin, 1982), p. 250.

[38]R. Beach, D. DeBeer, and S. R. Hartmann, Phys. Rev. A **32**, 3467 (1985).

[39]W. W. Chow, M. O. Scully, and J. O. Stoner, Jr., Phys. Rev. A **11**, 1380 (1975).

[40]S. Haroche, *High-Resolution Laser Spectroscopy*, edited by K. Shimoda (Springer, Berlin, 1976), p. 253.

[41]J. E. Rothenberg and D. Grischkowsky, Opt. Lett. **10**, 22 (1985).

[42]R. F. Loring and S. Mukamel, J. Chem. Phys. **83**, 4353 (1985).

[43]T. H. Einwohner, J. Wong, and J. C. Garrison, Phys. Rev. A **14**, 1452 (1976).

[44]At first glance it is not obvious that the third state in the superposition should be $|2\ 0\rangle_S$ and not $|2\ -2\rangle_S$. If the $|2\ -2\rangle$ state is used, a calculation of the induced dipole moment, $\mu_{\text{ind}} = \langle\psi|\mu|\psi\rangle$, leads to a mixed polarization state. Furthermore, if one considers the interaction of the E field with the atomic system in terms of optical quanta, it can be seen that the final state must be $|2\ 0\rangle_S$ in order to conserve angular momentum. If the atom is in an lcp field and absorbs a photon, the atomic system will change the projection of its angular momentum by -1 ($\Delta M_F = -1$). In order to return to a ground state energy level, the atomic system must return an lcp photon to the field, and the atomic angular momentum projection must return to its initial value. Consequently, the final state is $|2\ 0\rangle_S$, not $|2\ -2\rangle_S$.

[45]T. W. Ducas, M. G. Littman, and M. C. Zimmerman, Phys. Rev. Lett. **35**, 1752 (1975).